Characterization of Ice Mélange and its Implications to Terminus Stability at Helheim Glacier, Southeast Greenland

By

Steven Foga

Submitted to the Department of Geography and the
Graduate Faculty of the University of Kansas
in partial fulfillment of the requirements for the degree of
Master of Science

Dr. Cornelis J. van der Veen,
Chairperson

Committee members

Dr. Leigh A. Stearns

Dr. Stephen L. Egbert

Date defended: May 04, 2016

The Thesis Committee for Steven Foga certifies
that this is the approved version of the following thesis :

Characterization of Ice Mélange and its Implications to Terminus Stability at Helheim Glacier, Southeast Greenland

Dr. Cornelis J. van der Veen, Chairperson

Date approved: May 04, 2016

Abstract

Ice mélange, a conglomeration of icebergs and sea ice, persists in front of some marine-terminating glaciers. Depending upon local fjord geometry and other environmental conditions, an ice mélange can sometimes compact and jam. Here, the impact of the ice mélange on iceberg calving is assessed at a fast-moving glacier with a unique flow regime – Helheim Glacier, southeast Greenland (HG). Satellite remote sensing is used to quantify the ice mélange and the glacier terminus position, and additional ancillary data – wind speed, moorings, sea surface temperature (SST) and bed topography – are used to assess potential controls on iceberg calving. Iceberg jams were measured on a 2 to 35-day interval, but often did not correlate with the rate of calving. Isolated calving events were more likely during a jam, but most jams were in winter, when calving is most infrequent. At HG, SST and seasonality are the stronger drivers of iceberg calving.

Acknowledgements

Funding for this work was provided through National Science Foundation Grant ARC-0909373.

Contents

Chapter 1

Introduction

1.1 Outlet Glacier Dynamics

Over the past two decades, repeat measurements of the Greenland Ice Sheet's outlet glaciers indicate noticeable acceleration (e.g. Stearns & Hamilton, 2007; Howat et al., 2007; Moon et al., 2014) and thinning (e.g. Enderlin et al., 2014; Csatho et al., 2014; Murray et al., 2015), resulting in greater mass loss of the entire ice sheet (Velicogna, 2009; Zwally et al., 2011). The continuation of mass loss has serious implications for sea level rise, which has the potential to inundate low-lying coastal areas and adversely impact coastal populations (Church et al., 2013).

The environmental processes and subsequent mass loss mechanisms linked to glacier dynamics are relatively well known, but the contributions of each process to ice sheet mass loss at each individual glacier are difficult to accurately and precisely quantify. The difficulty of making these measurements is due to a combination of harsh climate conditions, relative remoteness of many of the field sites and expense of deploying instrumentation. Thus, numerical models are often used to recreate, describe, and predict glacier dynamics, and are often based upon empirical observation (e.g. Van der Veen & Whillans, 1989). Many of these models help identify the impact of ice mass loss mechanisms, which exist in two primary forms: liquid flux – ablation and runoff – and solid flux – iceberg calving. Using the aforementioned techniques, several studies identify ice mass

loss at several major outlet glaciers on the Greenland Ice Sheet to be driven primarily by surface melt, where above freezing air temperatures cause ablation and ice surface melt, resulting in ice thinning. Melt water drains into ice surface fissures, called crevasses, which can potentially expand the crevasses and weaken the glacier (Van der Veen, 2007; Van der Veen et al., 2011). Melt water can also drain through conduits called moulins, subsequently lubricating the bed and increasing glacier velocity (Zwally et al., 2002; Oerlemans, 2005; Bartholomew et al., 2010; Nick et al., 2012; Enderlin et al., 2014). One consequence of faster glacier movement may be more frequent iceberg calving (Van der Veen, 1996; Venteris, 1999; Thomas et al., 2003; Luckman et al., 2006), though other studies debate calving may be the trigger, and not the result of ice velocity increase (e.g. Hughes, 1986; Meier & Post, 1987; Joughin et al., 2004; Howat et al., 2005). The drivers of iceberg calving are more numerous and complex, and are described below.

1.2 Iceberg Calving

Iceberg calving can be triggered my multiple mechanisms, all of which vary geographically and are condition-specific; therefore a globally applicable calving law does not exist. In general, calving behavior is strongly linked with seasonal air temperature changes (e.g. Meier & Post, 1987; Luckman & Murray, 2005; Schild & Hamilton, 2013), where a combination of surface and basal crevasses driven by stretching and/or melt weaken the terminus to the point of calving (e.g. Benn et al., 2007). Calving can also be initiated at a marine-terminating glacier, known as a tidewater glacier, as a thinned terminus can become buoyant and calve (Meier & Post, 1987; Van der Veen, 2002; James et al., 2014). Buoyancy can also be regulated by the terminus position relative to the underlying bed conditions, where a grounded glacier terminus on a reverse bed slope can temporarily pin the terminus in place (Meier & Post, 1987; Pelto & Warren, 1991; Hughes, 1992; Van der Veen, 1996; Hanson & Hooke, 2000; Nick et al., 2010). Pinning points can also be caused by a combination of intermittent sediment deposits (e.g. Stearns et al., 2015), restrictive fjord geometry or shallow waters (e.g. Bassis & Jacobs, 2013). Calved icebergs may collect with sea ice and

become rigid, a physical trait known as an ice mélange. In constrained fjord conditions, the ice mélange may apply back pressure against the glacier terminus and temporarily suppress calving (e.g. Amundson et al., 2010).

Glacier flow and subsequent iceberg calving at tidewater glaciers can be much more rapid than ground-terminating glaciers (Meier et al., 2007; Joughin et al., 2008a; Nick et al., 2009), possibly due to warm ocean waters depleting mass and propagating crevasses at the glacier's terminus (Holland et al., 2008; Rignot et al., 2010; Motyka et al., 2011; Nick et al., 2012; Sutherland & Straneo, 2012). In terms of Greenland's tidewater glaciers, atmospheric influence via surface melt may be the dominant driver of iceberg calving (Nick et al., 2009; Enderlin & Howat, 2013; Enderlin et al., 2014; Davis et al., 2014). Furthermore, thinning and subsequent acceleration has been correlated more substantially with mass loss than calving (Bevan et al., 2015), though increased melt passed through subglacial channels could also trigger calving drive further mass loss (Slater et al., 2015).

Iceberg calving's impact on upflow glacier dynamics is highly debated. Some argue calving can trigger increased flow speeds (Amundson et al., 2008; Nick et al., 2009), increase calving by decreasing lateral resistance on the fjord walls (Joughin et al., 2004; Benn et al., 2007) or cause glacial earthquakes subsequently increasing flow rates (e.g. Nettles et al., 2008; Nettles & Ekström, 2010; Schild, 2011). Alternatively, calving may be a side effect of melt and thinning, as a well-lubricated bed increases flow and strain, thus increasing crevasses and triggering additional calving (e.g. Van der Veen, 2002).

1.3 Ice Mélange

Icebergs calved from tidewater glaciers are typically carried out of the fjord and into larger water bodies. Depending upon local conditions, such as water circulation and fjord geometry, icebergs are not always efficiently moved away from the terminus, and may persist in front of the terminus by freezing together or pinning against one another. This mixture of sea ice and calved icebergs is known as an ice mélange. Ice mélange is a well-known fixture of outlet glacier control in

Antarctica (e.g. Rignot & MacAyeal, 1998), and occurs at several tidewater glaciers in Greenland. Numerous findings assert that friction between the walls of the fjord and ice mélange could serve as potential points of ice velocity reduction near or around the glacier terminus (Pelto & Warren, 1991; Sohn et al., 1998; Reeh et al., 2001; Joughin et al., 2008b; Amundson et al., 2010; Howat et al., 2010; Amundson & Truffer, 2010; Walter et al., 2012; Sutherland et al., 2014; Peters et al., 2015). Several field campaigns have quantified the ice mélange using a number of techniques, including photogrammetry, synthetic aperture radar (SAR), lidar point clouds, and global positioning system (GPS) receivers. Amundson et al. (2010) make key observations at Jakobshavn Isbræ, West Greenland, where ice mélange has the ability to regulate calving by preventing icebergs from overturning after being calved from the glacier, which may reduce overall glacier flow velocity. Peters et al. (2015) examined Jakobshavn Isbræ's ice mélange over a single summer and found that ice mélange jams (begins to compress and slow) and releases (accelerates) immediately after calving events; similar short-term jam-and-release behavior has been successfully recreated in analogue models (Kuo & Dennin, 2013). These jams at Jakobshavn Isbræ persist for only an hour or less, and still have the ability to postpone some calving events (Peters et al., 2015). By tracking the movement of individual icebergs, Sutherland et al. (2014) found the ice mélange at Helheim Glacier, southeast Greenland generally moves in sync with the glacier terminus, but after moving 5-10 km away from the terminus will slow and compress; this compression region exists until $\sim$1 km away from the fjord outlet.

The ice mélange also exhibits seasonal behavior patterns. At Kangerdlugssuaq Glacier, East Greenland Sundal et al. (2013) note that the ice mélange is rigid and persists through the winter, and releases in the spring; this is similar to numerous West Greenland glaciers (Howat et al., 2010; Walter et al., 2012) whose ice mélange is also forced by sediment plumes released during the melt seasons (Chauché et al., 2014).

1.4 Objectives

With consideration to the complex nature of iceberg calving's contribution to glacier dynamics, and the evidence of temporary iceberg jamming events potentially playing a role on said mechanisms, the objective of this thesis is to quantitatively explore the relationship of iceberg calving to seasonality and to characterize the ice mélange at a fast moving tidewater glacier, namely Helheim Glacier, southeast Greenland (HG). HG loses the most mass of all the southeast Greenland outlet glaciers (Murray et al., 2015), has a unique flow regime (Stearns & Hamilton, 2007) and has a persistent ice mélange. Specifically, this thesis explores:

(a) glacier terminus behavior seasonally and inter-annually;

(b) if, when, and why terminus behavior correlates with the behavior of the ice mélange;

(c) how other environmental factors – wind, bed topography, sea surface temperature, and ocean temperature at depth – may also impact glacier terminus dynamics;

(d) all no-cost remote sensing data records to accomplish the aforementioned objectives.

1.5 Methods

The data used here are derived from satellite-borne remote sensing and ancillary data from weather stations, ocean mooring profiles and modeled observations. For the glacier terminus, both optical (Moderate Resolution Imaging Spectroradiometer (MODIS) Terra, MODIS Advanced Spaceborne Thermal Emission and Reflection Radiometer (ASTER), Landsat 5 Thermal Mapper (TM), Landsat 7 Enhanced Thermal Mapper Plus (ETM+), Landsat 8 Operational Land Imager (OLI)) and radar (Envisat Advanced Synthetic Aperture Radar (ASAR)) satellite images are used to create a record of terminus area, ice mélange area, terminus velocity, calving rate, and ice mélange rheology. Observations were collected between the years 2002 through 2014. The ASAR imagery are further used to derive characteristics of the ice mélange, such as velocity (when possible), iceberg

area, and iceberg distribution. Pre-compiled velocity maps (TerraSAR-X; Joughin et al. (2014)) are used when available. Four ancillary datasets: sea surface temperature from Advanced Very High Resolution Radiometer (AVHRR), maximum wind speed from a weather station, ocean mooring data (Harden et al., 2014) and two bed topography datasets (Bamber et al. (2013) and Morlighem et al. (2014)) are used to estimate potential impact on glacier terminus variability.

From these datasets, the significance of ice mélange and its ability to jam are considered in terms of where and when icebergs calve along the glacier terminus, denoted as *calving style*. The calving style, calving rate, and bed topography are compared with ice mélange jams, and how the physical systems interact with one another.

1.6 Thesis Format

This thesis is composed of an introduction, two journal articles, a conclusion and references. Journal article 1 is published in *Marine Technology Society Journal*, and covers the techniques used, associated error, and preliminary results of the glacier terminus and ice mélange quantification. Journal article 2 will be submitted to *Journal of Glaciology*, and examines the results and scientific implications of the data collected from 2002 through 2014.

Chapter 2

Application of Satellite Remote Sensing Techniques to Quantify Terminus and Ice Mélange Behavior at Helheim Glacier, East Greenland

PAPER

Application of Satellite Remote Sensing Techniques to Quantify Terminus and Ice Mélange Behavior at Helheim Glacier, East Greenland

AUTHORS

Steve Foga
Department of Geography, University of Kansas

Leigh A. Stearns
Department of Geology and Center for Remote Sensing of Ice Sheets (CReSIS), University of Kansas

C.J. van der Veen
Department of Geography, University of Kansas

ABSTRACT

Iceberg calving is an efficient mechanism for ice mass loss, and rapidly calving glaciers are often considered to be inherently unstable. However, the physical controls on calving are not well understood. Recent studies hypothesize that the presence of a rigid ice mélange (composed of icebergs, bergy bits, and sea ice) can reduce iceberg calving by providing "backstress" to the terminus. To test this hypothesis we use remote sensing techniques to construct a time series model of calving rate and size and composition of the adjacent ice mélange. We describe a semi-automated routine for expediting the digitization process and illustrate the methods for Helheim Glacier, East Greenland, using 2008 data. Ice velocities of the glacier terminus and ice mélange are derived with feature-tracking software applied to radar imagery, which is successfully tracked year-round. Object-based image analysis (OBIA) is used to inventory icebergs and sea ice within the ice mélange. We find that the model successfully identifies the calving rate and ice mélange response trends associated with seasonal increases in terminus retreat and advance and shows seasonal trends of ice mélange potentially providing seasonal backstress on the glacier terminus.

Keywords: glaciology, iceberg calving, object-based image analysis, feature tracking, ice mélange

Introduction

One of the major sources of uncertainty in predicting future rates of sea level rise due to climate change are the rapid changes affecting the flux of continental ice to the oceans via outlet glaciers, particularly glaciers that terminate in fjords or the open ocean (tidewater glaciers) (Vaughan et al., 2013). Negative mass imbalances in large parts of Greenland and Antarctica are being driven by recent accelerations of outlet glaciers (e.g., Rignot & Thomas, 2002; Rignot & Kanagaratnam, 2006) responding to unknown or poorly constrained perturbations in their boundary conditions. These changes have been observed by a variety of ground-based (e.g., Nettles et al., 2008; De Juan et al., 2010) and satellite instruments (e.g., Howat et al., 2007; Stearns & Hamilton, 2007), but the physical processes driving the changes are not well understood. In part, this is because coincident environmental changes, such as flow acceleration, retreat of the calving front, and changes in ice mélange geometry, make it difficult to separate forcings from responses. In addition, modeling studies aimed at identifying initial perturbations show that different forcings may lead to similar glacier response (Vieli & Nick, 2011). Consequently, predicting the response of the Greenland Ice Sheet's outlet glaciers to climate warming remains a large uncertainty in sea-level rise estimates.

Greenland's tidewater glaciers that terminate in fjords or the open ocean interact directly with the ocean. As such, their behavior may be sensitive to changes in ocean conditions as well as factors that affect their terminus buoyancy conditions (Bassis & Jacobs, 2013). Observations of glacier retreat, coincident with flow acceleration and thinning that extends ~50 km up-flow of the grounding line, suggest that changes occurring at glacier termini impact mass discharge of the whole glacier (e.g., Joughin et al., 2008a, 2008b; Payne et al., 2004). The physical processes driving observed rapid changes on these outlet glaciers are not well understood. In particular, whether changes in iceberg calving rates are the driver or

consequence of flow acceleration remains under debate. Recent studies suggest that an ice mélange at the terminus can control the rate of calving by imposing a backstress on the terminus (Sohn et al., 1998; Amundson et al., 2010). An ice mélange is a collection of icebergs, bergy bits, and sea ice, which aggregate in fjord constrictions. The ice mélange is potentially important to the dynamics at the glacier terminus, because it may provide seasonal backstress to the glacier front, resulting from compression and shearing of the mélange along the fjord, thus inhibiting calving (Sohn et al., 1998; Reeh et al., 2001; Amundson et al., 2010). Mélange rigidity and extent are two characteristics that have the potential to influence calving rates. Mélange rigidity depends upon the relative ratio of icebergs to sea ice. Sundal et al. (2013) observed that the amount of ice loss due to calving at Kangerlugssuaq Glacier increased during the summer months when the ice mélange was smaller in extent. They further noted that, when the mélange is composed of a higher percentage of icebergs, the mélange undergoes buckling and deceleration, synchronous with reduced iceberg calving. The mélange extent is modulated by the frequency of calving events, wind patterns, and ocean circulation (Joughin et al., 2008a, 2008b; Amundson et al., 2010). The role of mélange in modulating calving rates remains qualitative at best, however. For example, Schild and Hamilton (2013) attempted to find simple explanations for the observed patterns of advance and retreat on Helheim Glacier (due to air or ocean surface temperatures) but were unsuccessful, pointing to the need for additional information about terminus behavior.

To better examine the relationship of iceberg calving patterns at the ice-ocean interface, we developed a model of observations derived from remotely sensed datasets. We focus our model on Helheim Glacier, a fast-flowing tidewater glacier in East Greenland with a persistent ice mélange. Between 2002 and 2005, Helheim Glacier retreated >7 km, accelerated in terminus flow speeds from ~7,000 m a^{-1} to ~11,000 m a^{-1} and thinned by ~200 m (Stearns & Hamilton, 2007). The glacier has since slowed down (<8,000 m a^{-1}, Moon et al., 2012), although speeds have not returned to pre-2002 levels, and the terminus position shows considerable inter-annual variability (Schild & Hamilton, 2013).

In an attempt to fill critical data gaps, we developed a semi-automated technique to derive calving rate and mélange characteristics from synthetic aperture radar (SAR). Derived records include quantification of ice mélange extent and composition and allow us to compare ice surface velocity patterns to observations of terminus and mélange extent. In this study, only data from 2008 are used to test and validate our model. Extension to other years will be discussed in a future study. This work contributes to a current knowledge base of terminus change at Greenland's major outlet glaciers (Joughin et al., 2008a, 2008b; Seale et al., 2011; Schild & Hamilton, 2013).

Methods and Data

Terminus Area

We primarily use optical imagery from the Moderate Imaging Spectroradiometer (MODIS) instrument (Earth Observing System Data and Information System, 2009) to determine change in terminus and mélange extent. Both satellites in the MODIS network—Terra and Aqua—image the poles several times daily, making their temporal resolution ideal for analysis of dynamic features such as calving. Geolocation errors of MODIS are as small as 50 m at nadir but increase as the sensor points off-nadir, subsequently affecting co-registration (Wolfe et al., 2002). Therefore, this study uses only nadir images (1–2 times per day). MODIS scenes from the red and near-infrared bands are used and have a spatial resolution of 250 m. We analyze all possible MODIS images—from days 001 to 365—and use images where the glacier terminus is fully visible from the northern to southern edge of the fjord. Well-illuminated MODIS imagery is available from 1 March to 1 November of each year. The average data gap between MODIS scenes for the 2008 dataset is 6 days. We bridge data gaps caused by bad weather or solar illumination with imagery from the European Space Agency's Envisat Advanced Synthetic Aperture Radar (ASAR) geolocated imagery (https://earth.esa.int/web/guest/missions/esa-operational-eo-missions/envisat/instruments/asar). ASAR intensity images have a resolution of 10 m and a repeat track time of 35 days.

We primarily use Terra images in our analysis because it was launched in 1999 (Aqua was launched in 2002) and has a longer continuous record. Aqua images supplement missing or erroneous Terra images. Terra and Aqua acquire images within 2 h of one another and are processed using the same algorithms (NSIDC, 2014) and are delivered through an automatically generated text file. To expedite downloading HDF files, we developed a batch download tool written with the free-and-open-source programming language R (http://www.r-project.org/). Once acquired,

GeoTIFFs are extracted from the HDF file using the geospatial data abstraction library (GDAL, http://www.gdal.org/) and reprojected in the NSIDC North Polar Stereographic projection. Images are subset into the desired study area using shapefiles drawn in ArcGIS (Figure 1) and subset using batch processing in R.

We created a processing routine using R to efficiently analyze the daily MODIS images, relying on the *sp* (http://cran.r-project.org/web/packages/sp/index.html) and *raster* (http://cran.r-project.org/web/packages/raster/index.html) packages to display and subset the imagery. A pixel-level analysis determines the greatest difference between brightness values of pixels in each row of data and assigns a "pick" or digitization of the glacier terminus position. This method provides an initial guess for the location of the terminus, but results may be vulnerable to atmospheric effects and changes in illumination. Therefore, a graphical user interface was implemented using the *tcltk2* package (http://cran.r-project.org/web/packages/tcltk2/index.html), allowing the user to manually correct false picks (Figure 2). The functions controlled from within the GUI via mouse input are digitize, undo digitization, and delete digitization; functions available via interactive button controls are multiple color palette applications for imagery, imaging saving, and image discarding. Pixel-level digitization of the glacier terminus can be used to quantify the terminus area and identify regions across the terminus where calving events occur between sequential scenes. We determine terminus area from a fixed line behind the glacier terminus (Figure 1).

Uncertainties associated with quantifying the terminus area are derived from geo-location, co-registration, and digitization errors. Digitizing errors are dependent on the image resolution and repeatability of the manual corrections (when necessary). The uncertainty associated with resolution is quantified by calculating the terminus area using coincident high-resolution imagery (e.g., ASTER, Landsat 7 Enhanced Thematic Mapper Plus (ETM+), Landsat 8 OLI, and ASAR). For the 2008 dataset, we compare the terminus area measurements of seven temporally overlapping MODIS and ASAR images; the mean difference is 1.13 km^2 or 3.63% of the total area. We quantify the repeatability of the manual corrections by tracing the terminus from the same image 10 times and determining the standard deviation (after Schild, 2011), resulting in a standard deviation of 0.11 km^2.

Results of the terminus digitization are output into one comma-delimited file, containing total area and individual terminus measurements for each row of pixels.

FIGURE 1

Location map (inset) of Helheim Glacier, East Greenland, with the static target areas outlined by the dashed blue line (terminus area) and the solid red line (ice mélange). The background image is from the Landsat 8 Operational Land Imager (OLI) panchromatic band from 30 May 2013 (LP DAAC, 2008). (Color versions of figures available online at: http://www.ingentaconnect.com/content/mts/mtsj/2014/00000048/00000005.)

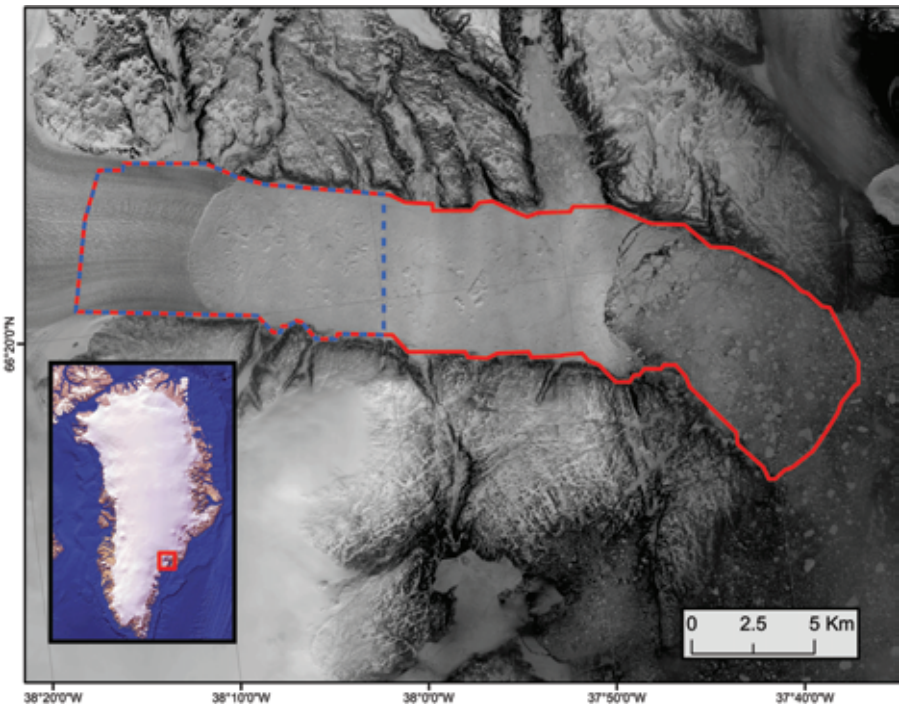

Ice Surface Velocity

We estimate ice velocity by applying a cross-correlation technique to sequential ASAR imagery. Velocity is measured in the terminus region over several epochs in 2008 using feature tracking software IMCORR (https://nsidc.org/data/velmap/imcorr.html). Sequential ASAR or high-resolution optical imagery (ASTER, Landsat ETM+ or OLI) can also be used (e.g., Stearns & Hamilton, 2007); since there are sufficient ASAR scenes in 2008, optical imagery is not used to

FIGURE 2

The *tcltk2* package allows for raster images to be digitized at the pixel level. The automated terminus prediction routine (A) is performed by finding the maximum difference between neighboring pixels in each row. This method is not accurate when clouds and shadows are present. The user-corrected image (B) allows correcting for any artifacts such as clouds or open water. The imagery is near infrared MODIS from 1 March 2008. Cell size is 250 m.

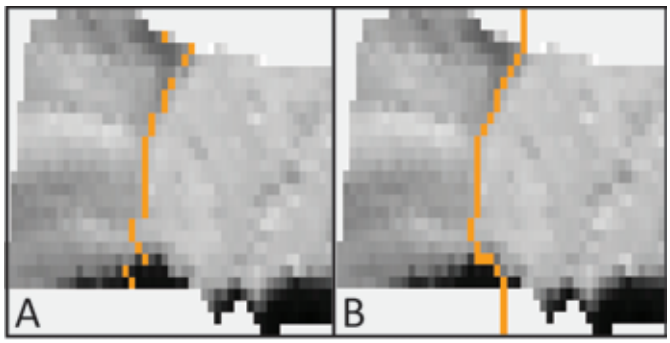

derive velocities in this study. Radar images are pre-processed with a low-pass filter to reduce noise and sharpen the desired ground features (after Scambos et al., 1992). We use a large 128 by 128 reference chip and a 64 by 64 search chip to encompass multiple features within each pass of the chips to ensure a better correlation at the cost of increased computation time. The 35-day repeat time of the sensor requires an offset of feature movement to be manually measured with ArcGIS and applied to IMCORR to reduce correlation error. The output product is a vector coordinate text file, which is converted into a raster image. To determine velocity at the terminus, 10 velocity grid values are averaged across the width of the glacier at an evenly spaced interval and are sampled from the points closest to the terminus. We determine the terminus position of the velocity grid to be at the more retracted position of the feature-tracked image pair.

Errors in feature tracking result from co-registration, resampling, and feature tracking mismatches. Co-registration issues are largely controlled by orbital corrections applied by ESA, but many features become more difficult to accurately track as the time separation between images increases. Using a technique similar to Bevan et al. (2012), we manually measure an identifiable feature tracked near the glacier terminus and compare the value to the IMCORR-derived value. We found the average error of our velocity maps derived in 2008 to be 0.24 m d^{-1}, similar to the Bevan et al. (2012) finding of 0.22 m d^{-1} for SAR imagery.

Calving Rate

The calving rate $\dot{c}$ is calculated from the difference between ice velocity at the terminus, U_t, and the change in position of the calving face, L, over time, t.

$$\dot{c} = U_t - \frac{dL}{dt}$$

It should be noted that the term "calving rate" refers to both iceberg calving and submarine melting: the position of the calving face is impacted by both of these processes.

Ice Mélange Area and Composition

We define ice mélange extent as the total area between the terminus of the glacier and the point where open water is visible. For the MODIS imagery, this extent is measured within the bounding boxes using a polygon delineation feature incorporated into our terminus picking tool (Figure 1). For the higher-resolution ASAR images, the extent is measured using manual polygon delineation in GIS software. The standard deviation of the MODIS ice mélange area is 5.85 km^2, which is determined by digitizing the same ice mélange 10 times in our picker. Error for ice mélange digitization is higher than terminus digitization due to a larger digitization footprint in the fjord than at the terminus. For ASAR, the error is 0.97 km^2, estimated by manually digitizing the same image 10 times in ArcGIS.

The ice mélange is composed of sea ice, icebergs, and bergy bits. We quantify the ratio and composition of the mélange in ASAR scenes by applying an object-based image analysis (OBIA) classification routine created and executed in Trimble's eCognition 8.7.2 Developer software (Figure 3). The key advantage to an object-based approach is the ability to analyze homogeneous clusters of pixels, which represent the whole extent of an object, instead of a pixel-based approach where only immediate neighbors are considered. To isolate individual icebergs from the surrounding sea ice, a multi-resolution segmentation algorithm is applied to the entire study area. Multi-resolution segmentation consists of three user-defined parameters. First, *scale* is a unitless measure indicating the maximum allowed homogeneity of a pixel cluster; the larger the desired objects, the larger the scale

FIGURE 3

Visual representation of the segmentation and classification process in eCognition. (A) is the original image once it has been subset and read into eCognition. (B) is the large segmentation. (C) is the sub-object segmentation of (B). (D) is the removal of the image border with high brightness and homogeneity thresholds. (E) is the classification of icebergs using the GLCM algorithm (blue); the background is classified (teal) to prevent misclassification in later steps. (F) is the result of classifying objects touching ≥75% of an iceberg. (G) is the final product, classifying all remaining objects as sea ice (red).

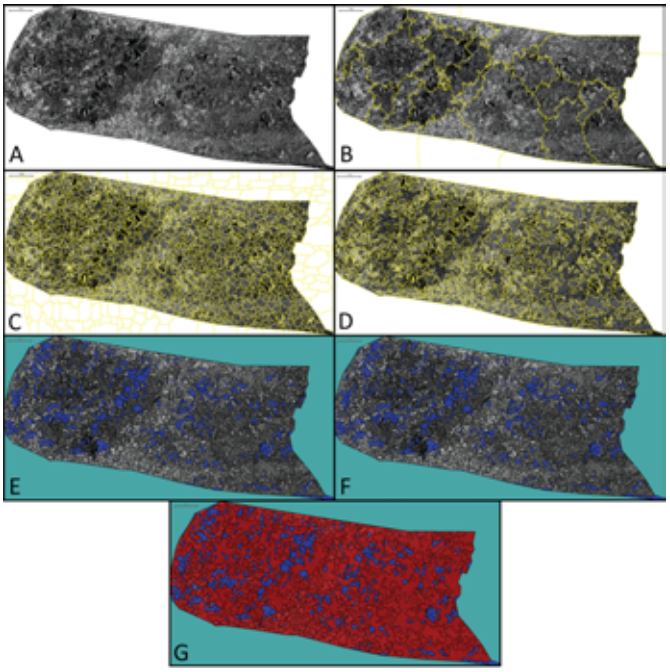

parameter (Trimble, 2012). Second, *shape* is defined on a scale of "round" to "thin and narrow". Third, *compactness* refers to the homogeneity of a pixel cluster. We start with a large-scale parameter of 200 (minimum ~3 km^2) to segment larger objects (Figure 3B) and then use a smaller-scale parameter of 30 (minimum ~0.01 km^2) to segment sub-objects within the larger super-objects (Figure 3C). The scale parameter can also be quantitatively determined using the estimation of scale parameter (ESP) tool, a plug-in available for eCognition software that incrementally tests scale parameters, and plots these against local variance and standard deviation (Drăguț et al., 2010). We find far fewer under- or over-segmented objects in our study area by using the ESP tool's results as a reference and manually adjusting the scale parameter in increments of 5 units until segmentation errors are minimized across the entire study area.

Classification of the resulting objects involves identifying area, shape, and radar return intensity characteristics of each object and reductively classifying each object until no more unclassified objects remain. Each object's classification is determined by assigning a score using several different weighted characteristics, known as a fuzzy membership. The mean score of the memberships results in an object being assigned to the classification most closely related to the assigned score. Six thresholds are implemented for classification: (1) Objects that were not efficiently segmented into smaller sub-objects are assumed to be sea ice due to its homogeneous appearance. Objects containing a large number of pixels (greater than 5,000 or 0.5 km^2) are assigned as sea ice, reducing the number of unclassified objects. (2) Icebergs return a higher intensity than the surrounding sea ice and are generally segmented into smaller objects. Fuzzy membership weights are applied to object intensity and area. (3) Open water returns a relatively low signal compared to neighboring objects. Weights for darker returns are classified as water. (4) Remaining portions of sea ice objects should be more heterogeneous than iceberg objects, though too small to be detected by the initial area parameter. Fuzzy membership is applied to a gray-level co-occurrence matrix (GLCM) algorithm, which searches in all directions to find objects that have a higher variation in texture (Figure 3E). (5) Objects sharing 75% or more of their border with an iceberg are likely interior portions of an iceberg that are not classified by the previous steps (Figure 3F). Fuzzy membership is applied to objects sharing a border with a classified iceberg. (6) All remaining objects are classified as sea ice (Figure 3G). The remaining objects are generally small, flat sections of sea ice.

The results of the classification are exported as both a thematic raster and a database containing each shape and classification. Both files are clipped in GIS software to eliminate glacier ice and open water before further analysis is performed.

We assess accuracy by generating 100 random points in ArcGIS and extracting the OBIA classifications and comparing those to the user-identified sea ice and iceberg classifications. We find the overall classification routine to be 88% accurate at identifying

icebergs. However, under-classification of icebergs is present under four different scenarios, ultimately resulting in a lower overall accuracy for measuring iceberg and sea ice area. First, icebergs will inherently be under-classified due to spatial resolution limitations of the ASAR imagery; as such, bergy bits and sea ice are considered one single classification. Second, sea ice clusters in open water form similar shapes and sizes as icebergs. We eliminate this issue by masking out open water before scenes are processed in eCognition. The third scenario is a symptom of signal response similarity between edges of icebergs and sea ice, which are incorrectly grouped into the same segment before classification occurs. Based on manual identification of each iceberg by shape and reflectance in one map, we estimate that this error occurs with ~10% of icebergs. The fourth scenario occurs when the signal response of an iceberg face is very similar to the surrounding sea ice. This typically leads to the majority of an iceberg's outer edges being correctly classified, but the remaining parts of the iceberg are assigned to sea ice. Based on examination of each iceberg in one map, we estimate that this error occurs within ~15% of icebergs.

FIGURE 4

Top: Results of the digitized terminus area and ice mélange extent. Raw values are shown as points (blue for terminus area and red for ice mélange). Raw values are smoothed and expressed as lines (blue for terminus area and red for mélange area). Values are normalized over each dataset, where 0 is the minimum measurement and 1 is the maximum measurement in 2008. Terminus area measurements outnumber ice mélange area measurements due to high cloud cover over the fjord. Bottom: Results of the ASAR feature-tracked terminus velocity (green) and calving rate (brown) measurements. Calving rate is averaged over the same epoch as a velocity measurement. A calving rate below the terminus velocity indicates that terminus is advancing while a calving rate exceeding terminus velocity means that the glacier terminus is in retreat. Feature-tracked velocities were not successfully generated for March to May.

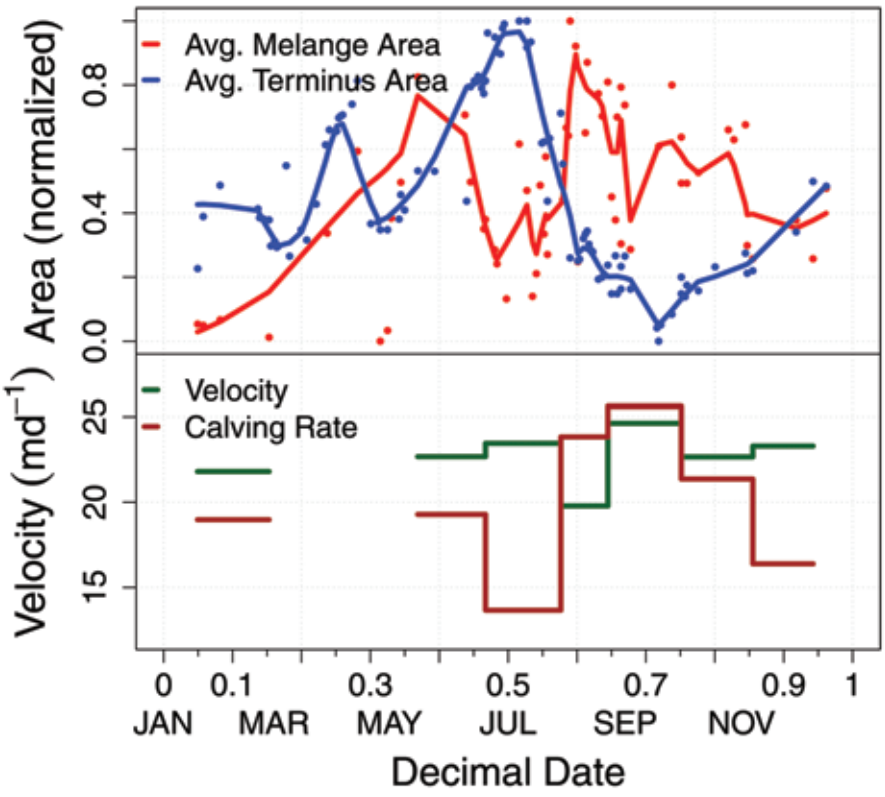

Results

Terminus Area and Calving Rate

Our method identifies several terminus advances in 2008 (Figure 4, top), consistent with the results reported earlier by Seale et al. (2011) and Schild and Hamilton (2013). The terminus generally advances between January and July, with short-lived periods of retreat in March and May. The terminus reaches its maximum area in July, before undergoing sustained retreat between July and September. The terminus retreats to a minimum area in September, which is later than any other annual retreat from 2001 to 2010 (Schild & Hamilton, 2013). After this large retreat in September, advance of the terminus area continues through the end of our 2008 record. Change in terminus area is greatest during the large advance-and-retreat cycle between July and September (Figure 4, top).

ASAR-derived ice velocities can be produced over the ice mélange and for a small region over the glacier trunk (Figure 5), but time separation or image resolution of the ASAR scenes prevents feature tracking on the trunk and margins. Radar intensity images may also inhibit feature tracking of small features due to noise and spatial resolution limitations.

Throughout most of 2008, the terminus velocity increases, interrupted by a marked slowdown in August and October-November (Figure 4, bottom). Compared to the seasonal changes in velocity observed in other years on Helheim Glacier (e.g., Bevan et al., 2012) and on other glaciers (e.g., Joughin et al., 2008a, 2008b, at

FIGURE 5

Velocity maps derived from ASAR scenes acquired on 18 January and 25 February 2008 (top), 14 May 2008 and 18 June 2008 (bottom). The black dotted line (denoted as Terminus Position 1) indicates terminus location in the reference image (18 January and 14 May), and the black solid line (Terminus Position 2) is the terminus position of the search image (25 February and 18 June). The white solid line is used to extract velocity profile; the corresponding velocity profiles are below each velocity map.

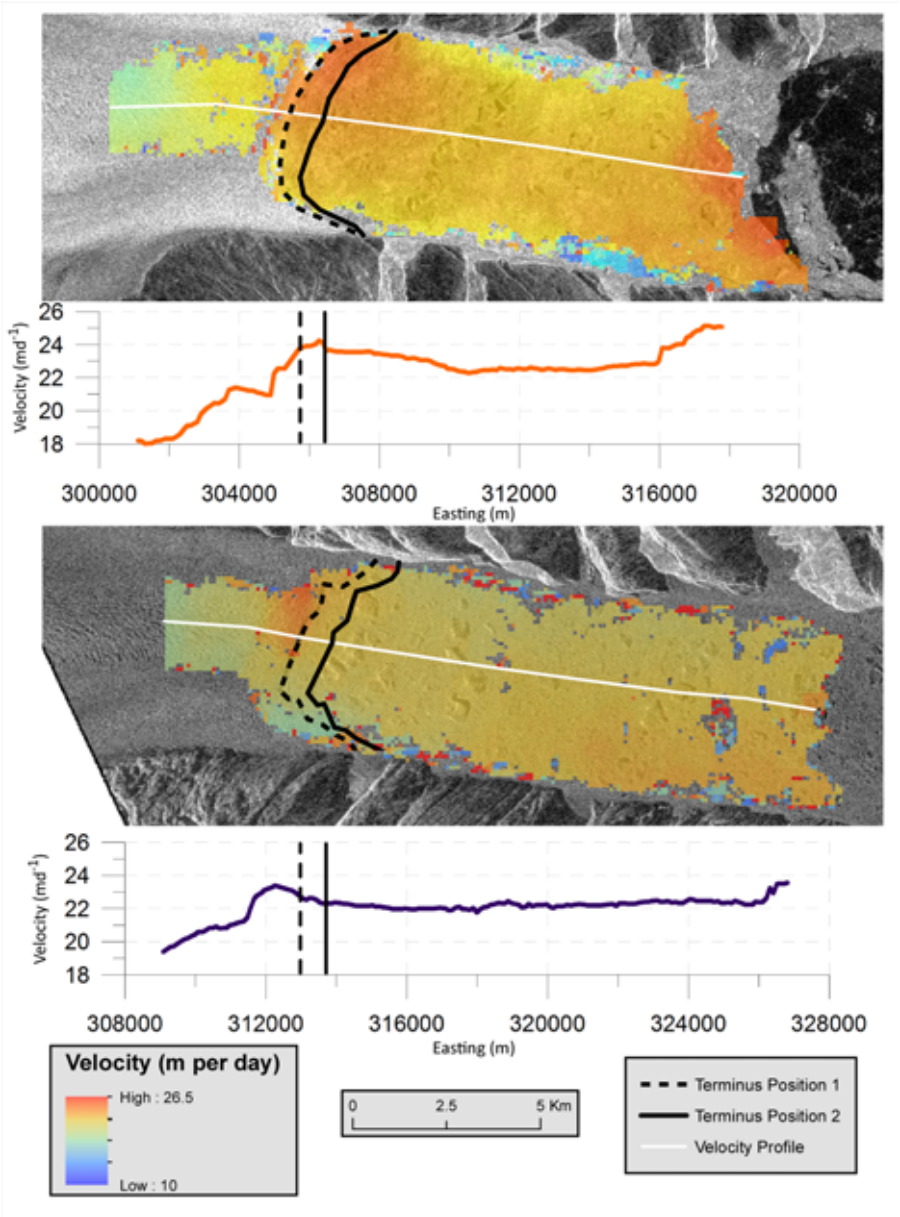

Jakobshavn Isbrae), ice velocity remains constant throughout 2008—the terminus velocity only has a standard deviation of 1.91 m d^{-1}.

Velocity of the ice mélange is measurable during the January-February and May-June measurements but is not measurable in subsequent measurements. Continuity of the ice mélange between ASAR acquisitions is essential in deriving ice velocities; results cannot be obtained using our method when the icebergs and sea ice move freely in the fjord.

Both ice velocity and calving rate reach a peak in August and September; because the calving rate exceeds the ice velocity, the glacier retreats during this time. For most of the year, ice velocity is larger than the calving rate, allowing the glacier terminus to advance.

Ice Mélange Extent

The extent of the ice mélange varies on short time scales throughout 2008 (Figure 4, top). Overall, the mélange slowly grows from January to May, although this trend is punctuated by short-lived, but large, periods of mélange reduction. As the glacier terminus advances between May and July, the mélange shrinks. Mélange extent is at its maximum in August, after which it steadily reduces in area until the end of the 2008 record. During periods of relatively large terminus area gain and loss (March and May to September; Figure 4, top), the ice mélange extent behaves inversely of terminus area. Periods of incremental change (January to February, April to May and September through December) reveal no consistent growing area trend between mélange and terminus area.

Ice Mélange Composition

The ice mélange composition is displayed in a segmented thematic map discerning both sea ice and ice mélange (Figure 6). The classification of icebergs allows us to determine the overall area covered by icebergs, which we divide by the area of sea ice to determine the ratio of icebergs to sea ice (Figure 7). The example in Figure 6 shows an ice mélange with consistently spaced icebergs through the first ~15 km of the fjord and increasing spacing toward the open ocean. Results from earlier and later months (when the calving rate is lower) show more distinct iceberg clustering at the glacier

FIGURE 6

An ASAR analysis image (top) used in eCognition to generate a thematic map (bottom) showing the distribution of large icebergs (purple), small icebergs, and sea ice (green). Once classification is complete, water is masked out of each image, leaving only large icebergs, small icebergs, and sea ice for analysis. Background image is Envisat ASAR from 23 July 2008.

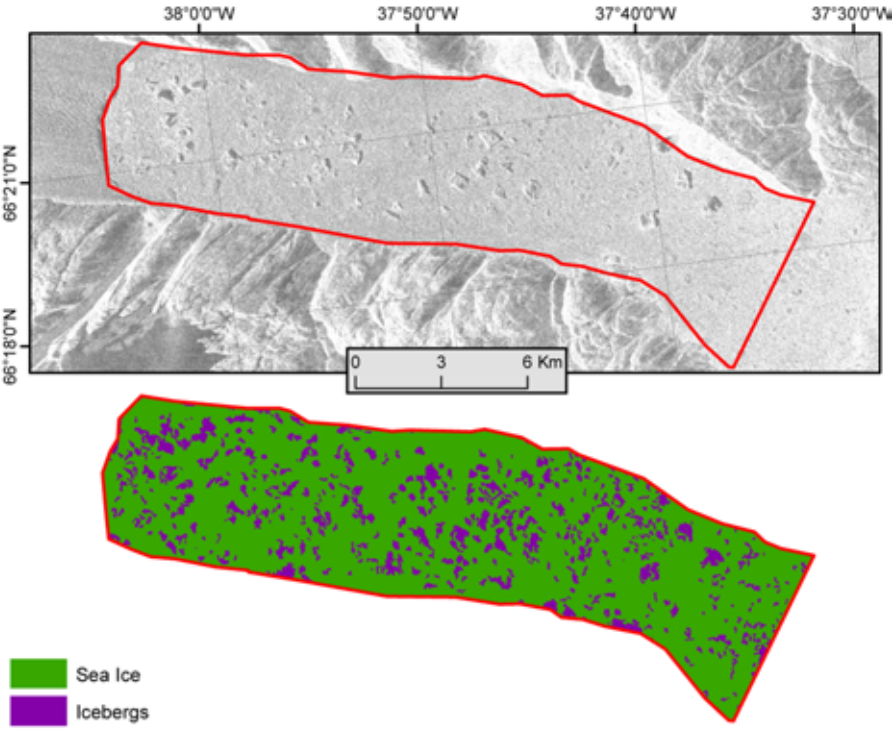

FIGURE 7

Ice mélange area (red points) plotted with the iceberg-to-sea ice ratio derived from the thematic OBIA maps.

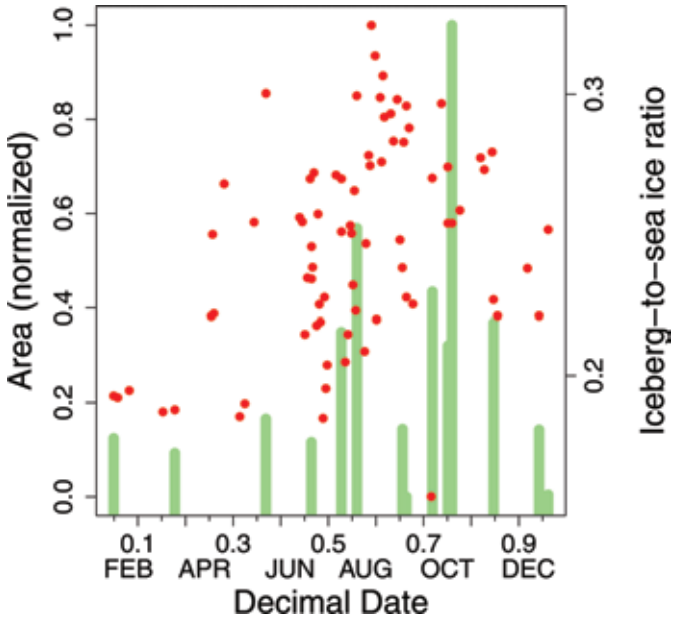

terminus, with icebergs spreading apart as they move down the fjord. The iceberg-to-sea ice ratio reflects this change in iceberg presence, as the ratio is higher in the summer (~0.25–0.3) and lower (~0.2) in winter, spring, and fall. During the winter and spring seasons, icebergs do not clear out of the fjord for at least 152 days. After the 11 July measurement, icebergs take as little as 12 days to exit the ice mélange, and icebergs continually move quickly until the end of the dataset.

Discussion

Role of Ice Mélange in Calving

An ice mélange is likely linked to calving processes through a complicated, and currently unproven, negative feedback cycle. Icebergs that are added to the mélange will impact the mélange rigidity and extent. However, a rigid mélange may provide substantial backstress to the glacier terminus, thus reducing calving rates. This feedback system is further complicated by other factors that control mélange composition (wind and air temperature) and calving rates (ice velocity and submarine melting rates).

Environmental factors at the ice-ocean interface that may control calving rates can originate from the ocean or atmosphere. Positive degree days can increase calving rates, as meltwater generated in surface crevasses could enhance fracture propagation and, thus, calving (Van der Veen, 1998; Vieli & Nick, 2011). Ocean temperatures and circulation patterns can impact submarine melt (Rignot et al., 2010; Rignot & Jacobs, 2002), which plausibly plays a role in both increased calving rate and ice mélange weakening. Warm water (>4°C) occupies Sermilik Fjord year-round, and estimates of submarine melt rates at the face of Helheim

Glacier are high (650 m a^{-1}) (Sutherland & Straneo, 2012). Our results, as well as those by Schild and Hamilton (2013), find no simple relationship between environmental controls and calving rates. Instead, we find that the calving rate is largely synchronous with changes in ice velocity, except at distinct periods in late summer, when large calving rates are likely controlled by environmental factors.

Mélange rigidity has the potential to modulate calving rates. Kuo and Dennin (2013) perform laboratory tests of the jamming ability of unsorted particles constrained in a trough and find that jamming primarily occurs when larger particles (icebergs) span the entire width of the trough and buckle to the sides. Observations in our study show that icebergs never span the entire width of the fjord, even during the highest iceberg-to-sea ice ratio occurrence (Figure 7). Additionally, the iceberg-to-sea ratio never reaches 0.4; the majority of solid material within the ice mélange is sea ice.

Calving rate and ice mélange extent are inversely related during the large advance-retreat epoch from May to September (Figure 4). In addition, mélange composition is not anomalous during this time of steady advance and then retreat (Figure 7). These observations strongly suggest that the ice mélange provides little to no backpressure during the summer and fall seasons. In addition, we were unable to derive mélange velocities during the summer and fall months, indicating that the mélange is not rigid and that icebergs are moving freely and are therefore untraceable in our approach.

In our results, ice mélange is slower than the glacier terminus in the winter and spring months of 2008, which is when the calving rate is at its lowest. Our results also show that terminus retreat begins after the ice mélange disintegrates in late June. This correlation may just be coincidental but does support the hypothesis that a rigid (thus slow) ice mélange reduces calving rate. Sundal et al. (2013) also observe winter mélange speeds that are slower than those at the glacier terminus—coincident with periods of reduced calving. Amundson et al. (2010) and Walter et al. (2012) observed similar calving reduction patterns in West Greenland.

Seasonal Variations

In 2008, the ice mélange varies in extent seasonally and weekly. In general, the mélange is smaller in the winter. It is also more rigid according to our ability to produce velocity estimates of the ice mélange by using a feature-tracking algorithm that only tracks translational motion. This rigid mélange does not change in size due to high winds. The mélange in the winter and early spring has a very low iceberg-to-sea ice ratio, presumably from a lower calving rate. These observations suggest that rigidity may be due to air temperature (as opposed to iceberg content).

During the spring, both the terminus and mélange grow in size—although both exhibit punctuated periods of retreat. These periods of retreat are coincident and short-lived, lasting only a few days for the mélange and a few weeks for the terminus. In early summer (mid-June to late July) ice velocity is high and calving rate is low, causing the glacier to advance. During this time, the mélange is reduced in size and contains few icebergs. The calving rate increases in late July until it exceeds the ice velocity and retreats. Retreat continues until September, continuously increasing the number of icebergs in the mélange. Mélange extent steadily decreases from mid-August to December, even though it presumably becomes more rigid with the increased number of icebergs.

The seasonality of the ice velocity plays a large role in the calving rate as well as the mélange speed. In 2008, Helheim Glacier steadily accelerated from January to October, with a period of deceleration in August. This deceleration caused the glacier to retreat because not enough ice was being supplied to the terminus to maintain a steady position. While the calving rate generally followed the ice velocity, a large decrease in calving rate in July occurred when velocity was relatively constant, suggesting that another variable impacted the calving rate during this time.

Model Success

The model is designed to define the significance of an ice mélange on calving events by providing insight to how icebergs and sea ice occupy the space within the fjord and how that variation coincides with iceberg calving rates. The model successfully identifies the calving rate and ice mélange response trends associated with seasonal increases in terminus retreat and advance. Icebergs are transported away from the ice mélange during times of increased calving, despite the increased flux deposited into the fjord. During times of terminus advance or a steady state in the winter months, the model shows the bulk of ice mélange never exceeds glacier flow, leading to the conclusion that the ice mélange has a role on calving rate variation at Helheim Glacier.

The primary shortcoming of the model is that it does not exhaustively determine all controls on the ice mélange. Factors such as wind, air temperature, sea surface temperature, and

tidal shift are not taken into consideration in the model. To simplify, we keep the scope of the study within the context of the ice mélange's control on calving and do not examine ice mélange controls. The other major shortcoming of the model is due to the resolution of the input datasets. Ice velocity measurements and ice mélange composition are bound to ASAR repeat times (35 days), leaving short-term velocity slowdowns and individual iceberg displacement unknown.

Summary

The combination of remote sensing techniques used in this study required the use of both commercial and free and open-source software, which extracted spatiotemporal glacier terminus area, ice mélange area, and ice mélange composition data from currently available remotely sensed data products. The use of a customized graphical user interface to identify and modify terminus location data and ice mélange extent provides a simple, fast, and accurate method of recording dynamics at the pixel level. The object-based method of classifying ice mélange is advantageous over a pixel-based approach, as object-based algorithms look not only at spectral differences between pixels but also at group homogeneous neighbors into objects. These objects provide additional dimensions (area, shape) to the classification process, making the discernment of ice types straightforward.

Acknowledgments

ASAR radar imagery provided by the European Space Agency under project C1P 16238; Landsat 8 data courtesy of the U.S. Geological Survey; the MODIS MOD09GQ data product was obtained through the online Data Pool at the NASA Land Processes Distributed Active Archive Center (LP DAAC), USGS/Earth Resources Observation and Science (EROS) Center, Sioux Falls, South Dakota (https://lpdaac.usgs.gov/data_access). Data from the Programme for Monitoring of the Greenland Ice Sheet (PROMICE) were provided by the Geological Survey of Denmark and Greenland (GEUS) on http://promice.org. Funding provided to LAS through National Science Foundation Grant ARC-0909373.

Corresponding Author:

Steve Foga
Department of Geography,
University of Kansas
1475 Jayhawk Blvd,
Lawrence, KS 66045
Email: steve.foga@gmail.com

References

Amundson, J.M., Fahnestock, M., Truffer, M., Brown, J., Lüthi, M.P., & Motyka, R.J. 2010. Ice mélange dynamics and implications for terminus stability, Jakobshavn Isbræ, Greenland. J Geophys Res. 115(F1):F01005. http://dx.doi.org/10.1029/2009JF001405.

Bassis, J.N., & Jacobs, S. 2013. Diverse calving patterns linked to glacier geometry. Nat Geosci. 6(10):833-6. http://dx.doi.org/10.1038/ngeo1887.

Bevan, S.L., Murray, T., Luckman, A.J., Hanna, E., & Huybrechts, P. 2012. Stable dynamics in a Greenland tidewater glacier over 26 years despite reported thinning. Ann Glaciol. 53(60):241-8. http://dx.doi.org/10.3189/2102AoG60A076.

de Juan, J., Elósegui, P., Nettles, M., Larsen, T.B., Davis, J.L., Hamilton, G.S., Stearns, L.A., & Forsberg, R. 2010. Sudden increase in tidal response linked to calving and acceleration at a large Greenland outlet glacier. Geophys Res Lett. 37(12):L12501. http://dx.doi.org/10.1029/2010GL043289.

Drăguţ, L., Tiede, D., & Levick, S.R. 2010. ESP: a tool to estimate scale parameter for multiresolution image segmentation of remotely sensed data. Int J Geogr Inf Sci. 24(6): 859-71. http://dx.doi.org/10.1080/13658810903174803.

Earth Observing System Data and Information System. 2009. Earth Observing System ClearingHOuse (ECHO)/Reverb, Version 10.X [online application]. Greenbelt, MD: EOSDIS, Goddard Space Flight Center (GSFC) National Aeronautics and Space Administration (NASA). URL: http://reverb.earthdata.nasa.gov.

Howat, I.M., Joughin, I., & Scambos, T.A. 2007. Rapid changes in ice discharge from Greenland outlet glaciers. Science. 315(5818):1559-61. http://dx.doi.org/10.1126/science.1138478.

Joughin, I., Howat, I., Alley, R.B., Ekstrom, G., Fahnestock, M., Moon, T., … Tsai, V.C. 2008. Ice-front variation and tidewater behavior on Helheim and Kangerdlugssuaq Glaciers, Greenland. J Geophys Res-Earth (2003–2012). 113:F01004. http://dx.doi.org/10.1029/2007JF000837.

Joughin, I., Howat, I.M., Fahnestock, M., Smith, B., Krabill, W., Alley, R.B., … Truffer, M. 2008. Continued evolution of Jakobshavn Isbrae following its rapid speedup. J Geophys Res-Earth (2003–2012). 113:F04006. http://dx.doi.org/10.1029/2008JF001023.

Kuo, C.C., & Dennin, M. 2013. Buckling-induced jamming in channel flow of particle rafts. Phys Rev E. 87(3):030201. http://dx.doi.org/10.1103/PhysRevE.87.030201.

Luckman, A., Murray, T., De Lange, R., & Hanna, E. 2006. Rapid and synchronous ice-dynamic changes in East Greenland. Geophys Res Lett. 33:L03503. http://dx.doi.org/10.1029/2005GL025428.

Moon, T., Joughin, I., Smith, B., & Howat, I. 2012. 21st-century evolution of Greenland outlet glacier velocities. Science. 336(6081):

576-8. http://dx.doi.org/10.1126/science.1219985.

NASA Land Processes Distributed Active Archive Center (LP DAAC). 2008–2009. MODIS MOD09GQ. In: USGS/Earth Resources Observation and Science (EROS) Center. Sioux Falls, South Dakota.

National Snow and Ice Data Center. 2014. NASA Distributed Active Archive Center (DAAC) at NSIDC, MODIS Data. URL: http://nsidc.org/data/modis/data_versions.html#temporal. Accessed 13 May 2014.

Nettles, M., Larsen, T.B., Elósegui, P., Hamilton, G.S., Stearns, L.A., Ahlstrøm, A.P., … Forsberg, R. 2008. Step-wise changes in glacier flow speed coincide with calving and glacial earthquakes at Helheim Glacier, Greenland. Geophys Res Lett. 35:L24503. http://dx.doi.org/10.1029/2008GL036127.

Payne, A.J., Vieli, A., Shepherd, A.P., Wingham, D.J., & Rignot, E. 2004. Recent dramatic thinning of largest West Antarctic ice stream triggered by oceans. Geophys Res Lett. 31:L23401. http://dx.doi.org/10.1029/2004GL021284.

Reeh, N., Thomsen, H.H., Higgins, A.K., & Weidick, A. 2001. Sea ice and the stability of north and northeast Greenland floating glaciers. Annals of Glaciology. 33(1):474-80. http://dx.doi.org/10.3189/172756401781818554.

Rignot, E., & Jacobs, S.S. 2002. Rapid bottom melting widespread near Antarctic ice sheet grounding lines. Science. 296 (5575):2020-3. http://dx.doi.org/10.1126/science.1070942.

Rignot, E., & Kanagaratnam, P. 2006. Changes in the velocity structure of the Greenland Ice Sheet. Science. 311 (5763):986-90. http://dx.doi.org/10.1126/science.1121381.

Rignot, E., Koppes, M., & Velicogna, I. 2010. Rapid submarine melting of the calving faces of West Greenland glaciers. Nat Geosci. 3(3):187-91. http://dx.doi.org/10.1038/ngeo765.

Rignot, E., & Thomas, R.H. 2002. Mass balance of polar ice sheets. Science. 297(5586):1502-6. http://dx.doi.org/10.1126/science.1073888.

Scambos, T.A., Dutkiewicz, M.J., Wilson, J.C., & Bindschadler, R.A. 1992. Application of image cross-correlation to the measurement of glacier velocity using satellite image data. Remote Sensing Environ. 42(3):177-86. http://dx.doi.org/10.1016/0034-4257(92)90101-O.

Schild, K.M. 2011. Terminus changes of tidewater outlet glaciers in Greenland: environmental controls and links to glacial earthquakes. M.S. thesis, University of Maine Orono. 100 pp.

Schild, K.M., & Hamilton, G.S. 2013. Seasonal variations of outlet glacier terminus position in Greenland. J Glaciol. 59(216): 759-70. http://dx.doi.org/10.3189/2013JoG12J238.

Seale, A., Christoffersen, P., Mugford, R. I., & O'Leary, M. 2011. Ocean forcing of the Greenland Ice Sheet: Calving fronts and patterns of retreat identified by automatic satellite monitoring of eastern outlet glaciers. J Geophys Res-Earth (2003–2012). 116: F03013. http://dx.doi.org/10.1029/2010JF001847.

Sohn, H., Jezek, K.C., & Van der Veen, C.J. 1998. Jakobshavn Glacier, West Greenland: 30 years of spaceborne observations. Geophys Res Lett. 25(14):2699-702. http://dx.doi.org/10.1029/98GL01973.

Stearns, L.A., & Hamilton, G.S. 2007. Rapid volume loss from two East Greenland outlet glaciers quantified using repeat stereo satellite imagery. Geophys Res Lett. 34(5). http://dx.doi.org/10.1029/2006GL028982.

Sundal, A.V., Shepherd, A., Van Den Broeke, M., Van Angelen, J., Gourmelen, N., & Park, J. 2013. Controls on short-term variations in Greenland glacier dynamics. J Glaciol. 59(217):883-92. http://dx.doi.org/10.3189/2013JoG13J019.

Sutherland, D.A., & Straneo, F. 2012. Estimating ocean heat transports and submarine melt rates in Sermilik Fjord, Greenland, using lowered acoustic Doppler current profiler (LADCP) velocity profiles. Ann Glaciol. 53(60):50-8. http://dx.doi.org/10.3189/2012AoG60A050.

Trimble. 2012. eCogniton Developer 8.7.2 Reference Book. München, Germany.

Van der Veen, C.J. 1998. Fracture mechanics approach to penetration of surface crevasses on glaciers. Cold Reg Sci Technol. 27(1):31-47. http://dx.doi.org/10.1016/S0165-232X(97)00022-0.

Vaughan, D.G., Comiso, J.C., Allison, I., Carrasco, J., Kaser, G., Kwok, R., … Zhang, T. 2013. Observations: Cryosphere. In: Climate Change 2013: The Physical Science Basis. Contribution of Working Group I to the Fifth Assessment Report of the Intergovernmental Panel on Climate Change [Stocker, T.F., Qin, D., Plattner, G.K., Tignor, M., Allen, S.K., Boschung, J., & Midgley, P.M., (eds.)], 317-82. Cambridge and New York: Cambridge Press.

Vieli, A., & Nick, F.M. 2011. Understanding and modelling rapid dynamic changes of tidewater outlet glaciers: issues and implications. Surv Geophys. 32(4-5):437-58. http://dx.doi.org/10.1007/s10712-011-9132-4.

Walter, J.I., Box, J.E., Tulaczyk, S., Brodsky, E.E., Howat, I.M., Ahn, Y., & Brown, A. 2012. Oceanic mechanical forcing of a marine-terminating Greenland glacier. Ann Glaciol. 53(60):181-92. http://dx.doi.org/10.3189/2012AoG60A083.

Wolfe, R.E., Nishihama, M., Fleig, A.J., Kuyper, J.A., Roy, D.P., Storey, J.C., & Patt, F.S. 2002. Achieving sub-pixel geolocation accuracy in support of MODIS land science. Remote Sensing Environ. 83(1): 31-49. http://dx.doi.org/10.1016/S0034-4257(02)00085-8.

Chapter 3

Characterization of iceberg calving and ice mélange behavior at Helheim Glacier, southeast Greenland

Characterization of iceberg calving and ice mélange behavior at Helheim Glacier, southeast Greenland

S. FOGA,[1] L.A. STEARNS,[2,3] C. J. VAN DER VEEN,[1] G.S. HAMILTON,[4] F. STRANEO,[5] D.A. SUTHERLAND[6]

[1] *Department of Geography, University of Kansas, Lawrence, KS, USA.*
E-mail: steve.foga@gmail.com
[2] *Department of Geology, University of Kansas, Lawrence, KS, USA.*
[3] *Center for Remote Sensing of Ice Sheets, University of Kansas, Lawrence, KS, USA.*
[4] *School of Earth and Climate Sciences, University of Maine, Orono, ME, USA.*
[5] *Department of Physical Oceanography, Woods Hole Oceanographic Institution, Woods Hole, MA, USA.*
[6] *Department of Geological Sciences, University of Oregon, Eugene, OR, USA.*

ABSTRACT. Ice mélange, a conglomerate of calved icebergs and sea ice, exists in some fjords adjacent to tidewater (marine-terminating) glaciers. Under certain conditions, ice mélange can become cohesive and jam, which may restrict the glacier terminus and subsequently reduce iceberg calving. In this study, we examine the impact of seasonality, ice mélange characteristics and other environmental forcings on iceberg calving at Helheim Glacier, southeast Greenland. Our observations are derived primarily from satellite observations collected between 2002 through 2014. We characterize glacier terminus behavior by its position, calving rate and calving style, and the ice mélange by its area, distribution of icebergs, size of icebergs, and velocity. We find that extended periods of ice mélange jamming (∼11-35 days) are tied more closely to cooler seasons (spring/fall/winter) and a high density of icebergs within 5 km of the glacier terminus. Longer duration ice mélange jams are not strongly tied to its rheology or environmental controls. Iceberg calving style and calving rate at Helheim Glacier are more closely tied to seasonality and sea surface temperature (SST) than the ice mélange's rheology, ice mélange rigidity, or basal topography, indicating that seasonal calving at Helheim Glacier is likely linked to surface melt.

INTRODUCTION

Mass loss from the Greenland Ice Sheet increased four-fold in the past two decades, resulting in a total contribution to global sea level rise of ∼0.4-0.7 mm y^{-1} (Shepherd and others, 2012; Enderlin and others, 2014; Csatho and others, 2014). Half of this mass loss came from the acceleration and retreat of marine-terminating glaciers (e.g. Moon and others, 2012), which are modulated by processes not well understood. The widespread retreat of Greenland's glaciers, and the coincidence with a period of oceanic and atmospheric warming, points toward a common climate driver (Csatho and others, 2014); however, details of both the forcing mechanism(s) and the response in outlet glacier dynamics are not fully understood (e.g. Vieli and Nick, 2011; Straneo and others, 2012).

Several recent studies conclude that changes in outlet glacier dynamics can be attributed to perturbations at the ice-ocean interface – through increases in submarine melt rates (Straneo and others, 2010; Johannessen and others, 2011; Sutherland and Straneo, 2012; Sciascia and others, 2013), weakening of an ice mélange (Straneo and others, 2013) or buoyant flexure of the glacier terminus (e.g. James and others, 2014). These mechanisms can lead to increased calving rates and retreat (e.g. Jenkins, 2011; Straneo and others, 2012; Slater and others, 2015). The controls on calving behavior are complex, and determining direct causality is not straightforward. In this study, we characterize the relationship of calving rate with seasonality, calving style and ice mélange behavior at Helheim Glacier (HG), in southeast Greenland.

Of the potential forcings at the ice-ocean interface, the ice mélange is arguably the least studied. An ice mélange may have implications to calving dynamics, as it has the potential to provide mechanical buttressing along fjord walls (Reeh and others, 2001; Amundson and others, 2010; Foga and others, 2014), control crevasse propagation (Amundson and Truffer, 2010), and alter energy transfer of calving icebergs (MacAyeal and others, 2012). Observations of ice mélange show that its rigidity changes over time, and therefore may have a variable impact on glacier calving rates. Using a ground-based radar interferometer, Peters and others (2015) find that the ice mélange at Jakobshavn Isbræ responds to individual calving events by compacting, jamming, and then relaxing, even when the ice mélange is at its most mobile. Results from radar and time-lapse camera observations show that the ice mélange does not offer much inherent resistance to the glacier terminus in the summer, but jams within 10 minutes following a large calving event, and then relaxes 40-60 minutes after (Peters and others, 2015). Similar calve-and-jam behavior occurs immediately after calving events at HG (Sutherland and others, 2014), and has been reproduced in an analogue model (Kuo and Dennin, 2013). At Store Gletscher, West Greenland, ice mélange removal coincides with an acceleration of the glacier terminus (∼1.5 m d^{-1}), yielding estimates of the ice mélange exerting ∼30-60 kPa of backstress against the terminus (Walter and others, 2012).

Our focus is on seasonal and inter-annual observations at HG. HG has an ever-present ice mélange, and has undergone many unique flow patterns over the past fifteen years: between 2002 and 2005, the terminus of HG experienced a rapid surface velocity increase of ∼4000 m a^{-1}, thinning ∼200 m at its terminus, and retreating ∼18 km^2 (Stearns and Hamilton, 2007). Since 2006, HG has remained relatively stable (Moon and others, 2012), yet has exhibited a pattern of thinning, thickening, and re-thinning (Csatho and others, 2014). Our study quantifies HG's terminus position and surface velocity, and examines the pattern of individual calving events, which we denote as *calving style*. We then quantify the ice mélange by its composition, surface velocity and extent, and compare its seasonal and inter-annual behavior with calving rate and calving style. These measurements span a 12-year period from 2002-2014.

METHODS

To quantify the impact of the mélange on calving behavior, we characterize both the ice mélange and glacier terminus using a combination of optical and radar satellite imagery. Here we focus specifically on the impact that seasonality, ice mélange composition, and ice mélange jams have on calving style and calving rate. We define *jams* as periods when the ice mélange is cohesive and moves more slowly than the glacier terminus. Note that the jams here are detected at an interval of several days to several weeks, meaning the more ephemeral jams observed by Peters and others (2015) cannot be detected here. We further explore the relationship of external forcings on HG terminus and ice mélange by using several ancillary datasets: sea surface temperature, wind speed, and ocean temperature.

Terminus Characterization

In this study, we use a semi-automatic technique to digitize the edge of the glacier terminus using each 250 meter pixel of Moderate Resolution Imaging Spectroradiometer (MODIS) Terra imagery (Foga and others, 2014), collected daily from 2002 through 2014; this per-pixel technique not only measures terminus position, but allows for geolocation of specific calving events.

To analyze calving style, we aggregate the terminus area data into five lateral transects (Fig. 1), where transects 1 and 5 are 750 m wide (3 pixels), and transects 2, 3, and 4 are 1000 m wide (4 pixels). The transect data are used to calculate change in terminus position in meters per day, and are discussed in terms of the entire time series, by season, and by year. Comparisons of the size and timing of calving events between transects are made using correlation coefficients (r).

Ice Mélange Characterization

We characterize the ice mélange by measuring the size and distribution of its icebergs, as well as the mélange extent and velocity. We define the mélange extent as the area of cohesive ice mélange, where no open water is visible, from the glacier terminus to the fjord edge. The ice mélange extent is manually delineated from MODIS imagery. We create an inventory of icebergs and sea ice within the ice mélange using object-based image analysis (OBIA) with Envisat Advanced Synthetic Aperture Radar (ASAR) imagery from 2002 through 2010, and Landsat 8 Operational Land Imager (OLI) imagery from 2013 through 2014. The OBIA technique allows us to retrieve icebergs statistics, specifically iceberg size and location. Further details about the OBIA methodology are outlined in Foga and others (2014). We analyze mélange characteristics within along-fjord zones (Fig. 1) to investigate how icebergs are distributed and how their spatiality may affect calving.

Terminus and Ice Mélange Velocity

We calculate terminus and ice mélange velocity by tracking surface features with image correlation software (Scambos and others, 1992) using imagery from ASAR, Landsat OLI, and the Advanced Spaceborne Thermal Emission and Reflection Radiometer (ASTER). Pre-compiled interferometry velocity maps are used when available (TerraSAR-X) (Joughin and others, 2011). To determine the calving rate, we average velocity values across the width of the glacier terminus. For each velocity epoch, we calculate the calving rate ($\dot{c}$) using the width-averaged velocity (u_M), and the width-averaged change in terminus position (L) between each velocity epoch (t):

$$\dot{c} = u_M - \frac{dL}{dt}. \quad (1)$$

Ancillary Datasets

We utilize ancillary datasets for sea surface temperature (SST) and wind speed to assess their impact on calving rate and ice mélange behavior. SST data is averaged from three spatially unique daily measurements from the Advanced Very High Resolution Radiometer (AVHRR) Optimum Interpolation dataset (Reynolds and others, 2007; Reynolds, 2009), which span the extent of Sermilik Fjord.

Wind speed data is from the University of Copenhagen's Sermilik Research Station at "Station Coast" established near the fjord at 65°40.8N, 37°55.0W, ∼75 km from the glacier terminus (Mernild and others, 2008), running from 2002-2012, and one weather station near HG in 2014-15. Oltmanns and others (2014) use the former dataset in conjunction with two other wind speed datasets to determine the change in fjord conditions and sea ice cover in response to downslope wind events (DWE), which are established as being ≥17.4 m s^{-1}. DWE affect the entire fjord when blowing in the directions between 270 degrees (East) and 20 degrees (South-southwest). Wind speed is captured every three hours; in our study, we use the maximum daily wind speed.

We use mooring data to assess the potential impact of ocean water temperatures on HG's terminus and/or ice mélange conditions. The data were acquired at three locations: Irminger Sea (100-600 m in depth), the Atlantic Ocean shelf adjacent to Sermilik Fjord (∼300 m), and Sermilik Fjord itself (100-500 m) (Harden and others, 2014).

Error Analysis

We assess the accuracy of the terminus position data by comparing temporally overlapping, higher-resolution images from Landsat 8 OLI, ASAR, and ASTER with our MODIS-derived record. The average error for the terminus area is 1.3

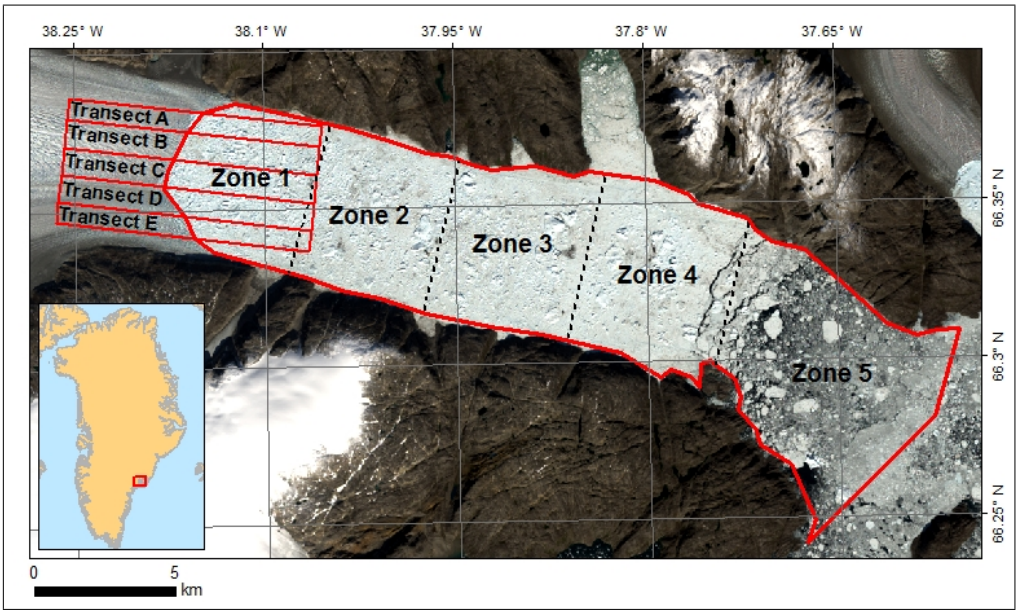

Fig. 1. The fjord is divided into zones (1-5) in order to analyze pattens in mélange rheology, and the terminus area is divided into transects (A-E) to analyze calving style. Zones and transects are overlain on a Landsat 8 OLI RGB composite image from 03 September 2013.

km^2 (4.1% of the study area). The ice mélange delineation error is 37.9 km^2 (22.7% of the study area) – likely due to ambiguity of ice mélange cohesion in MODIS imagery. Digitization repeatability errors are 0.1 km^2 for terminus area using MODIS imagery, and 5.9 km^2 (MODIS) and 0.9 km^2 (ASAR) for the ice mélange (Foga and others, 2014). Velocity errors are 0.24 m d^{-1} for ASAR scenes (Foga and others, 2014) and 0.82 m d^{-1} for OLI scenes. The error for TerraSAR-X derived velocities typically fall within 0.01 m d^{-1} to 0.05 m d^{-1}, depending upon proximity to shear margins (Joughin, 2002).

To assess the accuracy of identifying icebergs with the OBIA routine, we manually traced icebergs in one randomly selected image from ASAR and one from Landsat 8 OLI. The ASAR image classified with OBIA was 66.3% accurate compared to its manually digitized mask. Error is most prominent in the ASAR images where small icebergs (<∼2,200 m^2) are clustered together; this is the result of the algorithm sometimes aggregating adjacent, smaller icebergs into a single iceberg. This error has a noticeable effect when calculating the area of icebergs by zone, but does not significantly alter the distribution of the icebergs (Fig. 2). Results from the Landsat OLI digitization show better results than the ASAR object-based classification with an overall accuracy of 73.9%, and shows similar statistical fits as shown in Fig. 2. Overall, the accuracy of the iceberg area results from both datasets make its usefulness debatable, but iceberg distribution values were accurately obtained.

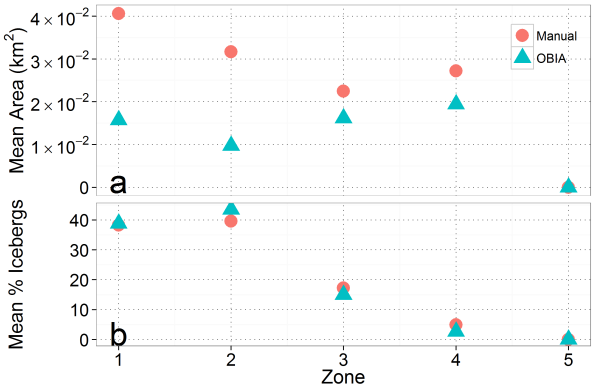

Fig. 2. Differences in zonal statistics for the single ASAR image, between the object-based classification ("OBIA") and the manually-digitized mask ("Manual"). The results show significant differences in categorizing iceberg size (**a**, r = -0.24), but show good agreement in mean percent of icebergs (**b**, r = 0.99).

RESULTS

Terminus and Mélange Extents

Both the terminus and ice mélange extents show clear seasonal signals (Fig. 3). In general, Helheim Glacier advances in the fall when the glacier is moving more slowly and begins to retreat in the spring when the glacier accelerates and calving rate increases. Not surprisingly, the ice mélange extent is inversely related to the terminus area – as the terminus retreats, the additional icebergs cause the mélange to extend both near the terminus and outward into the fjord. Calving rate varies closely with surface velocity (r = 0.75), and both correspond to the larger retreats and advances of the terminus. The calving rate became more stable after the 2002-2005 terminus retreat.

The ice mélange extent typically grows and shrinks along with seasonal variations in iceberg calving (Fig. 3d). A shorter ice mélange is observed during winter except during the late 2005/early 2006 winter; HG retreated ∼22 km^2 in summer 2005 and the mélange remains extensive throughout the winter 2005-06 (Fig. 3). During summer 2005, the terminus velocity and calving rate both exceeded 30 m d^{-1} (Fig. 3b,

c), simultaneously growing the ice mélange area to its second greatest extent measured (Fig. 3d). The ice mélange observations are partially explained by calving, but the ice mélange varies more irregularly and at a greater frequency than terminus area, terminus velocity or calving rate.

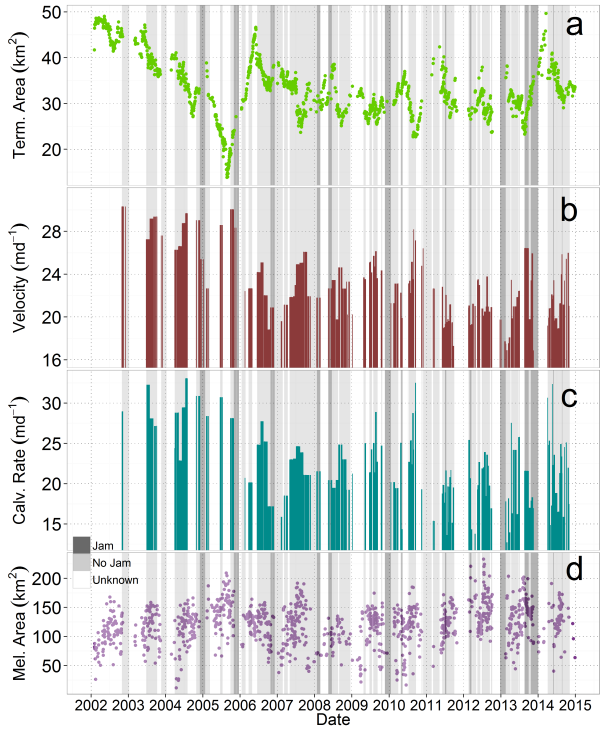

Fig. 3. a) Terminus area. **b**) Terminus velocity, where the width of the bars indicate the epoch of the measurement. **c**) Calving rate, where the width of the bars indicate the epoch of the measurement. **d**) Ice mélange area. Dark gray bars indicate an ice mélange jam observed within the surface velocity epoch; light gray indicates an ice mélange jam was not observed; white indicates unknown, as no data are present to measure ice mélange velocity.

Terminus and Mélange Velocity

Often usable ice mélange velocities cannot be produced due to its fast, nonlinear motion, particularly in the 35-day epochs of the ASAR imagery. The shorter epochs of the other velocity datasets (11 days for TerraSAR-X, and 2-16 days for Landsat OLI) mean less ice mélange movement, thus a greater chance to detect mélange compaction. Jams observed in the ASAR data occur exclusively in the late fall (as early as DOY 245) and winter, with an exception to 2008, when one jam occurred in the summer. Jams occur during all four seasons in the TerraSAR-X data, and during the late summer and fall in the Landsat OLI imagery (Fig. 3).

Iceberg jams, denoted by the dark gray bars in Fig. 3 and Fig. 5, occur nearly annually starting after the large series of terminus retreats in 2005. Jams occur under a variety of different conditions: when calving rate is positive and near zero (Fig. 3c); when ice mélange extent is fully extended and short (Fig. 3d); when SST is cold and warm (Fig. 4a); and when the wind speeds range from zero to a DWE (Fig. 4b). The ranges of data collected during jams versus all data are detailed in Table 1.

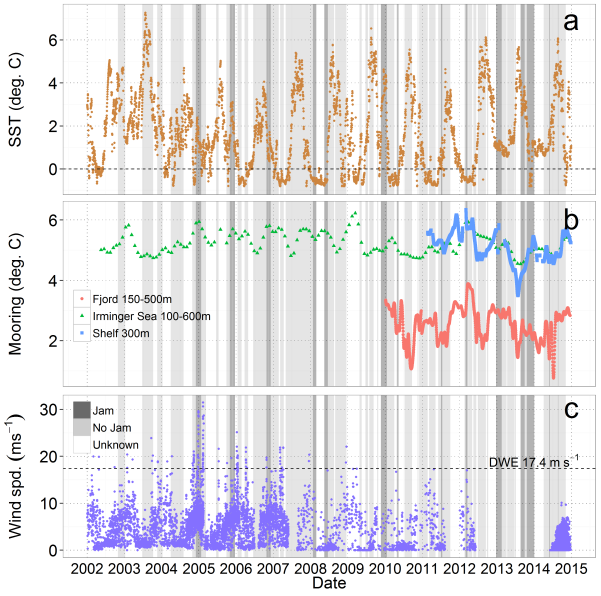

Fig. 4. a) Sea surface temperature. A black dashed line separates the freezing point of fresh water (0°C). **b**) Mooring data acquired in Sermilik Fjord (red), the Atlantic shelf immediately outside of Sermilik Fjord (green), and the surrounding Irminger Sea (blue). **c**) Wind speed data from Sermilik Fjord, filtered for wind directions between 270° (East) and 20° (South-southwest) degrees. A black dashed line separates the downslope wind event (DWE) established by (Oltmanns and others, 2014).

Ice Mélange Rheology

The mélange composition analysis is separated between two datasets: 2002 through 2010 (ASAR) and 2013 and 2014 (Landsat 8 OLI). High spatial resolution imagery is not available to derive mélange composition maps for 2011 and 2012. These datasets are analyzed separately, as ASAR and Landsat 8 OLI datasets were acquired at different intervals, and the ice mélange was often obfuscated by by cloud cover, reducing the time series density and creating distinctly different iceberg/sea ice ratio and iceberg area results that tell two different stories.

In the ASAR data (Fig. 5), the measured ice mélange characteristics – iceberg to sea ice ratio and mean iceberg size – are highly correlated ($r = 0.96$) and are inversely related to seasonal calving patterns: as HG retreats in mid-summer it produces numerous small icebergs that subsequently increase the overall area of the ice mélange. Conversely, in winter large icebergs are calved at infrequent intervals, and sea ice is less prevalent in the ice mélange. Of the seven ice mélange jams occurring between 2002 and 2010 (derived from both ASAR and TerraSAR-X data), iceberg distribution measurements were only possible from the five ASAR images. However, the distribution of iceberg/sea ice ratio and mean iceberg size measurements for jammed periods is nearly indistinguishable from a non-jammed ice mélange (Table 1). Regardless of conditions, the iceberg/sea ice ratio is always <1.0, indicating there is more sea ice and/or small iceberg bits (<∼2,200 m^2) than icebergs.

The Landsat 8 OLI data show a more dynamic view of the ice melange due to overlapping acquisition paths, but is sensitive to cloud cover, therefore rheology cannot always be analyzed at a consistent interval. Only two images in

2013 were cloud-free, but fifteen images in 2014 were cloud-free over the ice mélange. In the winter and early spring 2014, the ice mélange was often short (<5 km) and iceberg-filled (iceberg/sea ice ratio between 0.36 to 1.32), yielding results not found in the ASAR record. The iceberg/sea ice ratio and mean iceberg area went from maximum in mid April, and fell to minimum at the end of July. Only one of the five measured ice mélange jams coincide with an iceberg distribution measurement due to partial ice mélange obstruction by clouds. This particular observation falls in the summer (between DOY 233 and 235), has the smallest iceberg/sea ice ratio in 2014 (0.36) and when the ice mélange was fully extended, indicating that shorter-duration jams can occur during the summer.

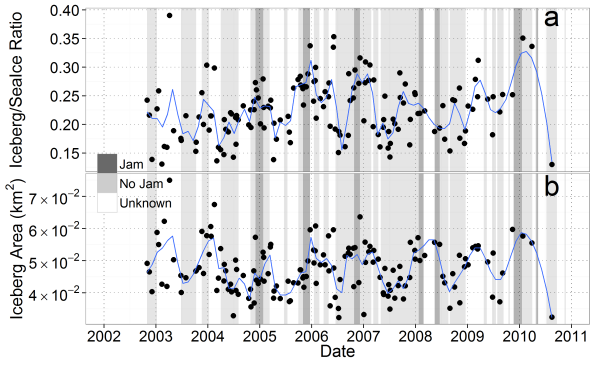

Fig. 5. Iceberg characteristics in Helheim Glacier's ice mélange, derived from ASAR images. **a**) The iceberg/sea ice ratio assumes that within a cohesive ice mélange, any object not detected as an iceberg is either sea ice or small, unresolvable icebergs. **b**) For all icebergs detected in each image, the area is calculated and represented as a mélange-wide mean. Gray bars represent the state of the ice mélange relative to the glacier terminus velocity.

To understand the seasonality of the ice mélange, we compare the iceberg/sea ice ratio and mean iceberg size by season and by distribution, which is determined by analyzing the data within five geographic zones of 5 km in width (Fig. 1). We calculate the standard deviation for each zone to account for the variability exhibited in the raw measurements. The concentration of icebergs is greatest at the terminus, and consistently decreases as it approaches the mouth of the fjord, regardless of season (Fig. 6a). During the summer, icebergs are distributed most evenly throughout the fjord compared to other seasons. There are more icebergs near the terminus in the winter than any other season, but these values can vary by ∼15% (Fig. 6b). The ice mélange was often shortest in winter months (sometimes never extending past zone 3), thus lowering the sample size in zones 4 and 5 during the winter. The icebergs measured in the winter tended to be larger in size in zone 5 (the mouth of the fjord) than the other seasons (Fig. 6c), but also vary greatly (Fig. 6d). Icebergs tend to be largest in winter and spring (Fig. 6c), which corresponds to the large, infrequent calving events observed during these seasons. Ice mélange characteristics during a jam are also plotted (without being aggregated by season), but show no unique characteristics.

To investigate the conditions under which ice mélange jams occur, the ice mélange statistics are filtered by incidence of jams. We find that jams occur when 20-35% of icebergs exist within zone 1 (32% average, Fig. 6a). Five of the seven jams occur exclusively in the winter. The overall distribution pattern suggests that jams occur when icebergs cluster near the terminus and tend not to happen in summer months. Icebergs also tend to be larger when jams occur, but not exclusively.

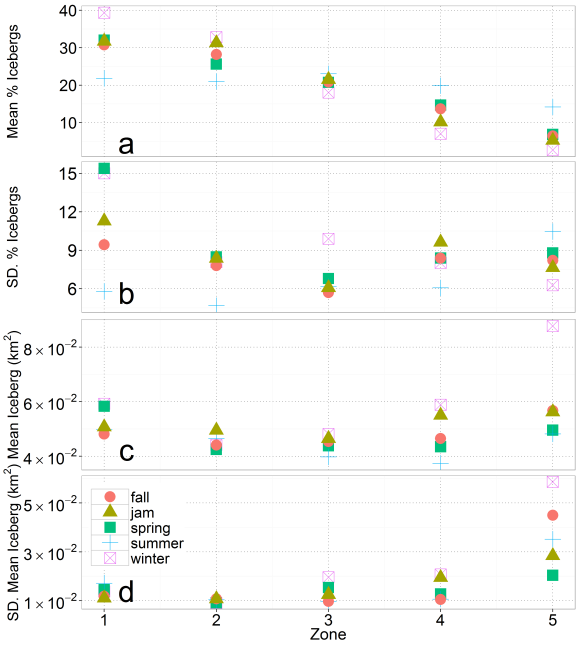

Fig. 6. a) Iceberg distribution throughout the ice mélange (refer to zone map in Fig. 1) aggregated by season and by periods of ice mélange jams for the 2002-2010 ASAR dataset. **b**) The standard deviations of the mean iceberg distributions vary between seasons, particularly near the terminus. **c**) Mean iceberg size, represented as area, of all icebergs within each zone, aggregated by season and by jam. Icebergs tend to start out larger near the glacier terminus (zone 1), but then become smaller as they move through the fjord, with exception of the fjord mouth (zone 5). **d**) The standard deviations of the mean iceberg size. The greatest variability is exhibited in zone 5.

Calving Style

Our analysis of the terminus area divided into transects (Fig. 1) show calving frequency is closely linked between adjacent transects, and correlations decrease as transects are farther apart (Fig. 7a). This suggests that calving events often span more than one transect, either as a single large iceberg, or multiple small icebergs. The correlation between any two transects is always positive, showing that the entire terminus generally advances and retreats as a single entity. Correlations are slightly higher between adjacent transects along the northern and central transects.

To further investigate the effect that ice mélange jams have on calving style, we subset the terminus data at coincident times of ice mélange jams (Fig. 7b). There are 74 samples collected during jams, making up only 5.1% of the entire terminus position record. All transects behave more randomly (r closer to 0) when the mélange is jammed, with the exception of Transects A and B, which are more closely correlated. Transect C (the centerline of glacier flow) and transect E (the southern edge of the terminus) have a nearly random correlation in the jam-only dataset, indicating the

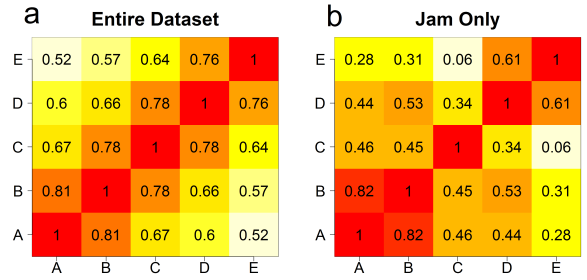

Fig. 7. a) A correlation matrix of each calving transect compared with one another for the entire 2002-2014 terminus position dataset. **b**) The correlation of each calving transect compared to one another coincident with all observed ice mélange jams.

size and location of calving events could be geographically isolated during ice mélange jams. The more random behavior of zones C, D and E are likely influenced by rising and falling tides, which have been observed to perturbate these zones, and directly impact glacier terminus velocity at HG (Voytenko and others, 2015), which may trigger iceberg calving.

DISCUSSION

Calving and Potential Ice Mélange Control

Amundson and Truffer (2010) suggest that the ice mélange impacts seasonal terminus geometry and iceberg calving style by preventing calving events that may otherwise have been triggered by terminus flotation, crevasse spacing, ice temperature, and/or terminus thickness. Seasonal variation in ice mélange rheology has been observed to some extent at other Greenland tidewater outlet glaciers: Seale and others (2011) note ice mélange cohesion beginning sometime after October and weakening ∼4 months later in February-March at Kangerdlugssuaq Glacier (KG), ∼330 km north-northeast of HG. They observed one instance of ice mélange clearing and re-forming 14 days later, which coincided with terminus retreat. Like KG, here we find HG has an always-present ice mélange, and jams occur in 2 to 35-day intervals, where jams last longer in winter and early spring months. Unlike KG, we observe that HG's terminus advances more than retreats during jams; the terminus retreated during jams only twice, but most jams occur during winter, which is when HG moves slower and calves less. Sometimes, ice mélange jams prevent icebergs from capsizing and separating from the glacier terminus (Amundson and others, 2010), which would still appear as an advancing terminus. The chance of this phenomenon increases with the size of the iceberg, and being grounded at the time of calving from the glacier (Amundson and others, 2010).

The timing of ice mélange rigidity could play a strong role in modulating iceberg calving. At HG, the ice mélange never completely disappears at HG, there is an observed reduction in the percent of icebergs next to the terminus between winter and spring seasons (Fig. 6a), which corresponds well to our results showing ∼70% of the 35-day jams occurred in winter (Fig. 5). Cassotto and others (2015) investigate the seasonal timing of ice mélange presence with calving events at Jakobshavn Isbræ. The ice mélange often relaxed and began accelerating above its mean velocity up to 20 days before a large calving event. Winter calving events and terminus advance were both correlated with variation in ice mélange behavior (Cassotto and others, 2015). Our observations at HG agree with these findings, as the icebergs within the ice mélange become more distributed along-fjord throughout the spring, summer, and fall, with summer being the most distributed and varying the least in the zones closest to the glacier terminus (Fig. 6a, b). Larger icebergs concentrated in zone 5 during the winter (Fig. 6c) may be grounded on a sill (Joughin and others, 2008). However, the impact of the sill on ice mélange stability could not be determined with our data.

During ice mélange jams, calving transects behave more independently, suggesting that large icebergs or across-width calving events are less common (Fig. 7b). Independence among zones may explain the high variation in calving rate during times of ice mélange jamming, as some parts of the terminus calve more than others. Calving style may appear independent due to the relatively small number of samples present during ice mélange jams, which are concentrated primarily in the winter. Furthermore, the terminus is almost always advancing during jams, implying that calving is reduced across the entire terminus relative to the summer and early fall calving style.

The large terminus retreat between 2002-2005 may be more closely linked with the above freezing SST values in 2002-2003. SST varies closely with seasonality, indicating warming air temperatures may be the greater driver of melt and subsequent iceberg calving at HG (Fig. 4). Irminger Sea waters were also warmer in 2002-2003 (∼6°C), indicating subglacial melting at the terminus could also be a factor increasing the calving rate and terminus velocity. Here we

Measured variable	Range of conditions	Mean value	Median value	% of all obs.	Date range
Terminus velocity	16.87 m d^{-1} to 29.04 m d^{-1}	22.89 m d^{-1}	22.47 m d^{-1}	**94.5%**	2002-2014
Calving rate	14.36 m d^{-1} to 30.87 m d^{-1}	20.13 m d^{-1}	20.68 m d^{-1}	**81.2%**	2002-2014
Ice mélange extent	37.99 km^2 to 220.15 km^2	121.50 km^2	122.0 km^2	**83.0%**	2002-2014
SST	0.40°C to 4.72°C	2.44°C	2.82°C	**89.3%**	2002-2014
Wind speed	0 m s^{-1} to 19.72 m s^{-1}	6.49 m s^{-1}	6.92 m s^{-1}	**82.6%**	2002-2012
Iceberg/sea ice ratio	0.176 to 0.295	0.242	0.252	**90.5%**	2002-2010 (ASAR)
Mean iceberg size	3.69x10^{-2} km^2 to 5.97x10^{-2} km^2	4.71x10^{-2} km^2	4.99x10^{-2} km^2	**90%**	2002-2010 (ASAR)
Iceberg concentration (zone 1)	20% to 35%	32%	31.44%	N/A	2002-2010 (ASAR)

Table 1. Observed ice mélange jamming conditions at Helheim Glacier compared to the total mean, median, and percent of all other environmental observations.

do not observe a clear trend of subsurface temperature fluctuation coinciding with changes in calving rate, even with a time lag applied (up to ±30 days), indicating that subsurface melting may not be a first-order driver of iceberg calving.

Controls on Ice Mélange

Based upon our set of ice mélange rheology maps (Fig. 5), an ice mélange's ability to jam is not necessarily dictated by size of icebergs nor the concentration of icebergs relative to sea ice. The density of icebergs (within the first 5 km of the terminus) is the most distinct feature we found related to our observed ice mélange characteristics.

Strong wind events may cause infrequent break up of the ice mélange during the winter, keeping the ice mélange short relative to summer and fall seasons. Oltmanns and others (2014) observe winds controlling the ice mélange when a single DWE passing through Sermilik Fjord reduced ice mélange cover by 29% in 2011. Similar observations have been made at Jakobshavn Isbræ (JI) (Cassotto and others, 2015), where warmer air temperatures could either be the cause (convection) or result (exposed warmer waters causing an increase in air temperature) of increased winds. However, little impact due to down-fjord events have been found at JI (Amundson and others, 2010). Likewise at HG, ice mélange velocity near the terminus does not increase with strong along-fjord winds (Sutherland and others, 2014), which agrees with our results pertaining to longer-term iceberg jams and DWE (Fig. 4c). Even DWE impacting ice mélange coverage in all of Sermilik fjord did not remove ice mélange immediate to HG (Oltmanns and others, 2014). Alternatively, the abrupt changes observed in ice mélange extent during winter could be influenced by tidal perturbations (e.g. Walter and others, 2012) rather than DWE.

Here we find the likelihood of ice mélange jams is most closely linked with lower SST/air temperature. Often in winter, the waters at the surface are below freezing (Fig. 4a). Waters at depth are always above freezing, and are even warmer during the winter when they are not cooled by glacier runoff (Straneo and others, 2011). Here we observe ice mélange is more often jammed in the winter, and for longer durations than other seasons; 2002 and all of 2003 were an exception, as there was an absence of ice mélange jams and SST was above freezing, indicating that SST have more of an impact on ice mélange rigidity. Runoff from the summer season has the ability to cool subsurface waters (Straneo and others, 2011; Sciascia and others, 2013), but never below freshwater nor ocean water freezing points. Considering that long-term jams are not observed during the summer, we therefore assume iceberg calving and SST have greater control on ice mélange rigidity than subsurface water temperatures. However, SST does not perfectly explain these events: while no long-term ice mélange jams were observed during 2002-03, and the mean SST was 1.18°C, a sustained 54-day jam in winter 2012-13 occurred while SST was above freezing (0.92°C avg.), indicating that SST is not the exclusive driver of ice mélange jamming.

The Role of Bed Topography on Calving

Overall terminus stability is thought to be modulated by the glacier bed. However, recent models show that glaciers do not always stabilize on topographic bedrock highs; Nick and others (2010) found the bed of marine-terminating glaciers is most stable on reverse slopes or in shallow waters, and areas of instability may be prevalent on reverse bed slopes (e.g. Weertman, 1974; Thomas, 1979). Stability may also be impacted by the flotation (or ungrounding) of the glacier terminus (e.g. Van der Veen, 1996; Amundson and Truffer, 2010). A glacier with a floating ice tongue may be more susceptible to calving than a fully grounded glacier due to loss of stability provided by the bed (Meier and Post, 1987), which was observed after HG's retreat in 2005 (Joughin and others, 2008).

To test HG's terminus stability based on bed topography, we aggregate all 1400 terminus positions tracked between 2002 though 2014 (Fig. 8), referred to here as *frequency*. There is only one value assigned to each row for any given image. The spatial distribution of these pixels follows a normal Gaussian curve, where the peak frequency exists near the center of the profile at all three transects. We compare the terminus frequency data with two bed topography datasets: a 1 km resolution bed elevation dataset compiled with radar observations by Bamber and others (2013), and a 250 m resolution bed elevation dataset with combined radar and mass conservation techniques (Morlighem and others, 2014). In this comparison, we assume that a higher terminus position frequency indicates a location of greater terminus stability.

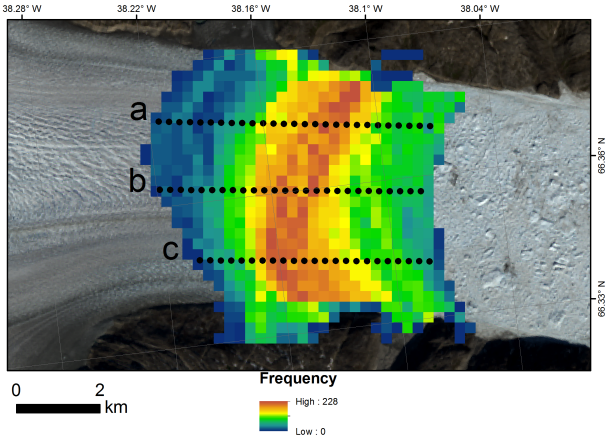

Fig. 8. Samples of terminus position frequency for the entire dataset (2002-2014) are taken from three different along-flow transects. Each sample is 250 m apart. Profile b is at the center of the glacier, and Profiles a and c are ∼2km away from b. The samples are shaded to show distribution of the 1400 unique days of terminus position data.

Terminus frequency and bed elevation datasets are sampled at 250 m intervals (Fig. 9). Each of the three frequency profiles behave similarly, but peak at slightly different points in relation to the bed topography. To examine the contribution of ice mélange and/or bed topography impacting the terminus position, we filter the data for periods concurrent with an ice mélange jam, and plotted in relation to bed elevation (Fig. 9).

The attempt to correlate calving style with bed topography (Fig. 9) shows that the terminus position relative to the bed during jams strongly resembles periods of non-jams; however, the two selected bed topography datasets largely disagree, making it difficult to draw any serious conclusions about the true physical relationship between calving style and bed topography. If the Bamber and others (2013) bed is more accurate, the bed may be the primary control on terminus

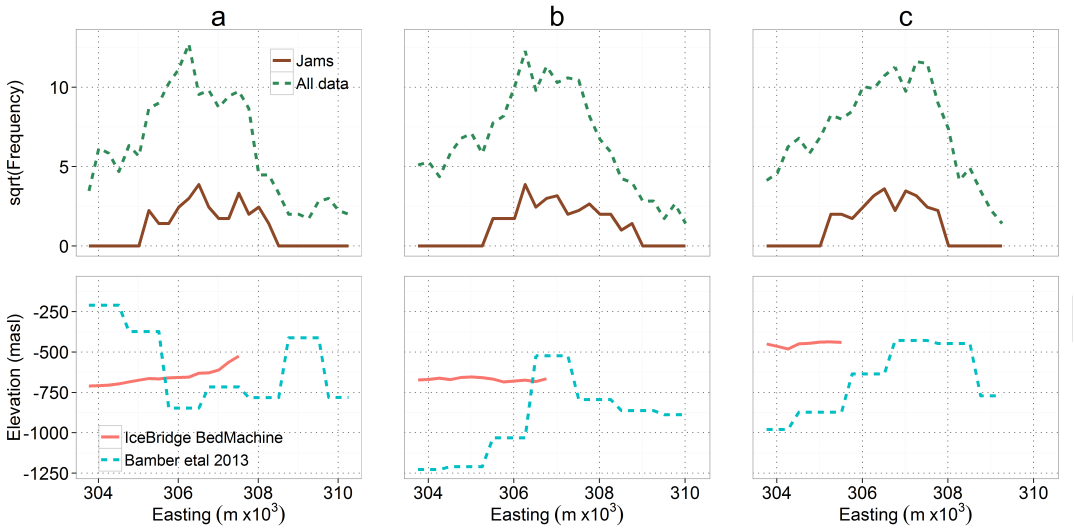

Fig. 9. Profiles of terminus position frequency graphed against two unique bed topography datasets (top). The 'All data' terminus position frequencies (dashed green) correspond to Fig. 8. The 'Jams' frequencies (solid brown) are filtered for coincident periods of ice mélange jamming. Both frequency datasets are square root transformed to exaggerate detail. The cooresponding bed topography – IceBridge BedMachine (solid red) and Bamber and others (2013) (dashed blue) notably disagree, and are shown at the bottom.

position, as the terminus is most frequently on a reverse bed slope in the center of flow, while the terminus near the fjord walls rest on plateaus. A reverse bed slope combined with fast flow and a relatively deep bed could be a driver for rapid calving (e.g. Pelto and Warren, 1991). However, the frequency of the terminus position does not differ greatly between transects, and is stable on a reverse bed slope, indicating that continuous calving could be restrained by another force, such as the ice mélange.

Variations in Calving Style

We test for the potential controls on calving style by comparing them to our derived environmental variables shown in Fig. 3. Here we define *calving style* as the behavior of the terminus between one transect and another (1). For each year, we calculate the correlation coefficients between transects, and then calculate the correlation coefficients for each season. The results of the correlations between the environmental variables and calving style yielded nearly random coefficients (r = -0.08 to 0.11), except for SST (r = 0.36). The transects behave more congruently during years when SST was above freezing for the majority of the winter than years when SST was below freezing. Likewise, in seasons where one or more transect pairs were inversely correlated, SST was an average of 0.58°C, which is low relative to the dataset-wide mean of 2.44°C. This observed behavior could be due to surface runoff from warmer temperatures, hydrofracturing surface crevasses and inhibiting calving across the entire terminus (e.g. Van der Veen, 1998). Increased melt at the surface could also induce faster breakup of the ice mélange, causing it to quickly move out of the fjord, thus relieving any potential pressure on the glacier terminus, subsequently allowing more calving to take place across the entire terminus. However, we do not observe a subsequent increase in calving rate nor uniformity of calving style when the ice mélange becomes un-jammed, indicating that it is likely a second-order control on calving style, if at all.

CONCLUSION

By exhausting the satellite remote sensing record and several ancillary datasets, we characterized iceberg calving behavior in relation to the sustained ice mélange in front of Helheim Glacier, southeast Greenland (HG). We used these derived characteristics to examine: 1) the ice mélange's ability to jam based upon its composition, size, and season; and 2) the implications of ice mélange jamming's impact to terminus position, calving rate and calving style at HG.

Ice mélange jams were rarely observed in longer 35-day acquisition epochs; they were primarily detected in the fall and winter starting in 2005. Jams < 35 days are sporadically detected with the 11-day epochs, and a single 2-day epoch in summer 2014, implying that ice mélange jam duration is linked to seasonality. The 2-day epoch in 2014 was observed in the summer with a fully extended ice mélange (∼26 km), indicating that a longer ice mélange could be a key mechanism in driving short-term jams, which has been noted in other field-based research. The proximity of icebergs to the glacier terminus are linked with jamming potential, as 30% (±12%) of icebergs during jams are concentrated within the first 5 km of the fjord, and decrease as they move away from the terminus (Fig. 6a). On average, a jam consisted of an ice mélange covering ∼73% of the fjord and an iceberg/sea ice ratio of 0.242, which was relatively dense in terms of our 2002-2010 ASAR observations, but not so for the 2013-2014 observations. The distribution of iceberg size remained constant relative to the seasonal trends, showing iceberg size is not a conclusive variable for characterizing the ice mélange's ability to jam at HG, though our iceberg size dataset was only ∼66% accurate.

In terms of ice mélange jams as a potential control on calving, our dataset comparisons showed that ice mélange jams occurred during a wide range of conditions (Table 1).

HG's terminus was almost always advancing during ice mélange jams, indicating calved icebergs could be held in place by the ice mélange to inhibit further calving, similar to the findings of Amundson and others (2010), but may be coincident with decreased melt during the winter. Overall calving behavior in the context of this dataset are more explainable through seasonality and SST, as calving rate increases when the seasons become warmer. Ice mélange jams were not correlated with our calving rate measurements.

By separating the terminus into five along-flow transects, we quantified how and where HG's terminus calves, and how it varies across space and time; we defined this as *calving style*. The variation among transects increases as distance between transects becomes greater, yet all transects were nearly always correlated positively with one another (Fig. 7). Overall, seasonality and SST were the clearest signals in terms of explaining calving style variation. Many peaks and troughs in our mooring data did not coincide with calving rate or terminus position changes, indicating that submarine melt may be a second-order control on calving. Likewise, the ice mélange and coincident jams occurred under a range of observed environmental and glacier terminus conditions, but often occur for month-long periods during the winter, indicating that ice mélange also has a second-order control on calving at HG, but more so in winter. Smaller calve-and-jam scenarios observed by field-based research find the ice mélange and iceberg calving closely interact, but these trends were not apparent in our results.

ACKNOWLEDGEMENTS

Thanks to Ian Joughin (U. Washington-APL) for additional MEaSUREs InSAR surface velocity data. ASAR radar imagery provided by the European Space Agency under project C1P 16238. The MODIS MOD09GQ and ASTER data products were obtained through the online Data Pool at the NASA Land Processes Distributed Active Archive Center (LP DAAC), USGS/Earth Resources Observation and Science (EROS) Center, Sioux Falls, South Dakota (https://lpdaac.usgs.gov/data_access/). Landsat 8 OLI data are courtesy of the U.S. Geological Survey. Wind speed data provided by the University of Copenhagen. Funding provided to L.A. Stearns through National Science Foundation Grant ARC-0909373.

REFERENCES

Amundson J and Truffer M (2010) A unifying framework for iceberg-calving models. *J. Glaciol.*, **56**(199), 822–830 (doi: 10.3189/002214310794457173)

Amundson J, Fahnestock M, Truffer M, Brown J, Lüthi M and Motyka R (2010) Ice mélange dynamics and implications for terminus stability, jakobshavn isbræ, greenland. *J. Geophys. Res.: Earth Surface (2003–2012)*, **115**(F1) (doi: 10.1029/2009JF001405)

Bamber J, Griggs J, Hurkmans R, Dowdeswell J, Gogineni S, Howat I, Mouginot J, Paden J, Palmer S, Rignot E and others (2013) A new bed elevation dataset for greenland. *The Cryosphere*, **7**(2), 499–510 (doi: 10.5194/tc-7-499-2013)

Cassotto R, Fahnestock M, Amundson J, Truffer M and Joughin I (2015) Seasonal and interannual variations in ice melange and its impact on terminus stability, jakobshavn isbræ, greenland. *J. Glaciol.*, **61**(225), 76–88 (doi: 10.3189/2015JoG13J235)

Csatho BM, Schenk AF, van der Veen CJ, Babonis G, Duncan K, Rezvanbehbahani S, van den Broeke MR, Simonsen SB, Nagarajan S and van Angelen JH (2014) Laser altimetry reveals complex pattern of greenland ice sheet dynamics. *Proceedings of the National Academy of Sciences*, **111**(52), 18478–18483 (doi: 10.1073/pnas.1411680112)

Enderlin E, Howat I, Jeong S, Noh M, Angelen J and Broeke M (2014) An improved mass budget for the greenland ice sheet. *Geophys. Res. Lett.*, **41**(3), 866–872 (doi: 10.1002/2013GL059010)

Foga S, Stearns L and van der Veen C (2014) Application of satellite remote sensing techniques to quantify terminus and ice mélange behavior at helheim glacier, east greenland. *Marine Technology Society Journal*, **48**(5), 81–91 (doi: 10.4031/MTSJ.48.5.3)

Harden BE, Straneo F and Sutherland DA (2014) Moored observations of synoptic and seasonal variability in the east greenland coastal current. *J. Geophys. Res.: Oceans*, **119**(12), 8838–8857 (doi: 10.1002/2014JC010134)

James TD, Murray T, Selmes N, Scharrer K and OLeary M (2014) Buoyant flexure and basal crevassing in dynamic mass loss at helheim glacier. *Nature Geoscience*, **7**(8), 593–596 (doi: 10.1038/ngeo2204)

Jenkins A (2011) Convection-driven melting near the grounding lines of ice shelves and tidewater glaciers. *Journal of Physical Oceanography*, **41**(12), 2279–2294 (doi: 10.1175/JPO-D-11-03.1)

Johannessen OM, Korablev A, Miles V, Miles MW and Solberg KE (2011) Interaction between the warm subsurface atlantic water in the sermilik fjord and helheim glacier in southeast greenland. *Surveys in geophysics*, **32**(4-5), 387–396 (doi: 10.1007/s10712-011-9130-6)

Joughin I (2002) Ice-sheet velocity mapping: a combined interferometric and speckle-tracking approach. *Ann. Glaciol.*, **34**(1), 195–201 (doi: 10.3189/172756402781817978)

Joughin I, Howat I, Alley R, Ekstrom G, Fahnestock M, Moon T, Nettles M, Truffer M and Tsai V (2008) Ice-front variation and tidewater behavior on helheim and kangerdlugssuaq glaciers, greenland. *J. Geophys. Res.: Earth Surface (2003–2012)*, **113**(F1) (doi: 10.1029/2007JF000837)

Joughin I, Smith B, Howat I and Scambos T (2011, updated 2014) Measures greenland ice velocity: selected glacier site velocity maps from insar, version 1. [ecoast-66.50n]. *Boulder, Colorado, USA: NASA DAAC at the National Snow and Ice Data Center*, **10** (doi: 10.5067/MEASURES/CRYOSPHERE/nsidc-0481.001), accessed 2016-02-08

Kuo C and Dennin M (2013) Buckling-induced jamming in channel flow of particle rafts. *Physical Review E*, **87**(3), 030201 (doi: 10.1103/PhysRevE.87.030201)

MacAyeal D, Freed-Brown J, Zhang W and Amundson J (2012) The influence of ice melange on fjord seiches. *Ann. Glaciol.*, **53**(60), 45–49 (doi: 10.3189/2012/AoG60A027)

Meier M and Post A (1987) Fast tidewater glaciers. *J. Geophys. Res.: Solid Earth (1978–2012)*, **92**(B9), 9051–9058 (doi: 10.1029/JB092iB09p09051)

Mernild S, Hansen B, Jakobsen B and Hasholt B (2008) Climatic conditions at the mittivakkat glacier catchment (1994–2006), ammassalik island, se greenland, and in a 109-year perspective (1898–2006). *Geografisk Tidsskrift-Danish Journal of Geography*, **108**(1), 51–72 (doi: 10.1080/00167223.2008.10649574)

Moon T, Joughin I, Smith B and Howat I (2012) 21st-century evolution of greenland outlet glacier velocities. *Science*, **336**(6081), 576–578 (doi: 10.1126/science.1219985)

Morlighem M, Rignot E, Mouginot J, Seroussi H and Larour E (2014) Deeply incised submarine glacial valleys beneath the greenland ice sheet. *Nature Geoscience*, **7**(6), 418–422 (doi: 10.1038/ngeo2167)

Nick F, Van der Veen C, Vieli A and Benn D (2010) A physically based calving model applied to marine outlet glaciers and implications for the glacier dynamics. *J. Glaciol.*, **56**(199), 781–794 (doi: 10.3189/002214310794457344)

Oltmanns M, Straneo F, Moore G and Mernild S (2014) Strong downslope wind events in ammassalik, southeast greenland. *Journal of Climate*, **27**(3), 977–993 (doi: 10.1175/JCLI-D-13-00067.1)

Pelto M and Warren C (1991) Relationship between tidewater glacier calving velocity and water depth at the calving front. *Ann. Glaciol.*, **15**, 115–118

Peters I, Amundson J, Cassotto R, Fahnestock M, Darnell K, Truffer M and Zhang W (2015) Dynamic jamming of iceberg-choked fjords. *Geophys. Res. Lett.*, **42**(4), 1122–1129 (doi: 10.1002/2014GL062715)

Reeh N, Thomsen H, Higgins A and Weidick A (2001) Sea ice and the stability of north and northeast greenland floating glaciers. *Ann. Glaciol.*, **33**(1), 474–480 (doi: 10.3189/172756401781818554)

Reynolds R (2009) What's new in version 2. Noaa/ncdc rep., online; Accessed 2015-09-27

Reynolds R, Smith T, Liu C, Chelton D, Casey K and Schlax M (2007) Daily high-resolution-blended analyses for sea surface temperature. *Journal of Climate*, **20**(22), 5473–5496 (doi: 10.1175/2007JCLI1824.1)

Scambos T, Dutkiewicz M, Wilson J and Bindschadler R (1992) Application of image cross-correlation to the measurement of glacier velocity using satellite image data. *Remote Sensing of Environment*, **42**(3), 177–186 (doi: 10.1016/0034-4257(92)90101-O)

Sciascia R, Straneo F, Cenedese C and Heimbach P (2013) Seasonal variability of submarine melt rate and circulation in an east greenland fjord. *J. Geophys. Res.: Oceans*, **118**(5), 2492–2506 (doi: 10.1002/jgrc.20142)

Seale A, Christoffersen P, Mugford R and O'Leary M (2011) Ocean forcing of the greenland ice sheet: Calving fronts and patterns of retreat identified by automatic satellite monitoring of eastern outlet glaciers. *J. Geophys. Res.: Earth Surface (2003–2012)*, **116**(F3) (doi: 10.1029/2010JF001847)

Shepherd A, Ivins E, Geruo A, Barletta V, Bentley M, Bettadpur S, Briggs K, Bromwich D, Forsberg R, Galin N and others (2012) A reconciled estimate of ice-sheet mass balance. *Science*, **338**(6111), 1183–1189 (doi: 10.1126/science.1228102)

Slater D, Nienow P, Cowton T, Goldberg D and Sole A (2015) Effect of near-terminus subglacial hydrology on tidewater glacier submarine melt rates. *Geophys. Res. Lett.*, **42**(8), 2861–2868 (doi: 10.1002/2014GL062494)

Stearns L and Hamilton G (2007) Rapid volume loss from two east greenland outlet glaciers quantified using repeat stereo satellite imagery. *Geophys. Res. Lett.*, **34**(5) (doi: 10.1029/2006GL028982)

Straneo F, Hamilton GS, Sutherland DA, Stearns LA, Davidson F, Hammill MO, Stenson GB and Rosing-Asvid A (2010) Rapid circulation of warm subtropical waters in a major glacial fjord in east greenland. *Nature Geoscience*, **3**(3), 182–186 (doi: 10.1038/ngeo764)

Straneo F, Curry RG, Sutherland DA, Hamilton GS, Cenedese C, Våge K and Stearns LA (2011) Impact of fjord dynamics and glacial runoff on the circulation near helheim glacier. *Nature Geoscience*, **4**(5), 322–327 (doi: 10.1038/ngeo1109)

Straneo F, Sutherland D, Holland D, Gladish C, Hamilton G, Johnson H, Rignot E, Xu Y and Koppes M (2012) Characteristics of ocean waters reaching greenland's glaciers. *Ann. Glaciol.*, **53**(60), 202–210 (doi: 10.3189/2012AoG60A059)

Straneo F, Heimbach P, Sergienko O, Hamilton G, Catania G, Griffies S, Hallberg R, Jenkins A, Joughin I, Motyka R and others (2013) Challenges to understanding the dynamic response of greenland's marine terminating glaciers to oceanic and atmospheric forcing. *Bulletin of the American Meteorological Society*, **94**(8), 1131–1144 (doi: 10.1175/BAMS-D-12-00100.1)

Sutherland D and Straneo F (2012) Estimating ocean heat transports and submarine melt rates in sermilik fjord, greenland, using lowered acoustic doppler current profiler (ladcp) velocity profiles. *Ann. Glaciol.*, **53**(60), 50–58 (doi: 10.1029/2006GL028982)

Sutherland D, Roth G, Hamilton G, Mernild S, Stearns L and Straneo F (2014) Quantifying flow regimes in a greenland glacial fjord using iceberg drifters. *Geophys. Res. Lett.*, **41**(23), 8411–8420 (doi: 10.1002/2014GL062256)

Thomas R (1979) The dynamics of marine ice sheets. *J. Glaciol.*, **24**, 167–177

Van der Veen C (1996) Tidewater calving. *J. Glaciol.*, **42**(141), 375–385

Van der Veen C (1998) Fracture mechanics approach to penetration of bottom crevasses on glaciers. *Cold Regions Science and Technology*, **27**(3), 213–223 (doi: 10.1016/S0165-232X(98)00006-8)

Vieli A and Nick F (2011) Understanding and modelling rapid dynamic changes of tidewater outlet glaciers: issues and implications. *Surveys in geophysics*, **32**(4-5), 437–458 (doi: 10.1007/s10712-011-9132-4)

Voytenko D, Stern A, Holland DM, Dixon TH, Christianson K and Walker RT (2015) Tidally driven ice speed variation at helheim glacier, greenland, observed with terrestrial radar interferometry. *J. Glaciol.*, **61**(226), 301–308 (doi: 10.3189/2015JoG14J173)

Walter J, Box J, Tulaczyk S, Brodsky E, Howat I, Ahn Y and Brown A (2012) Oceanic mechanical forcing of a marine-terminating greenland glacier. *Ann. Glaciol.*, **53**(60), 181–192 (doi: 10.3189/2012AoG60A08)

Weertman J (1974) Stability of the junction of an ice sheet and an ice shelf. *J. Glaciol.*, **13**, 3–11

Chapter 4

Conclusion

This thesis examined iceberg calving and potential influences from ice mélange and environmental factors at Helheim Glacier, southeast Greenland (HG). The information was disseminated through two peer-reviewed manuscripts, where the first manuscript examined the satellite remote sensing techniques used to quantify iceberg calving, ice mélange rheology and ice surface velocity, and the second paper examined the specific patterns of iceberg calving and potential environmental influences in relation to the ice mélange jams.

The results from the first paper showed through the use of object-based image analysis (OBIA), ice mélange rheology could be systematically measured using a workflow derived from empirical characteristics of the icebergs, specifically shape, size, and texture. The glacier terminus was digitized on a per-pixel level in MODIS imagery, which yielded data quantifying glacier retreat/advance and the spatiality of iceberg calving along the terminus. Measuring both glacier terminus and ice mélange surface velocities in 2008 revealed that the ice mélange has the ability to "jam" or move slower than the glacier terminus, indicating that the ice mélange rigidity may impact iceberg calving events at HG.

The second paper used the methods applied in the first paper, expanded the scope to years 2002 through 2014, and examined possible controls of iceberg calving at HG. Additional ancillary datasets were incorporated to help determine contribution and causality to calving behavior,

specifically wind speed, bed topography, moorings and sea surface temperature (SST). The ice mélange rheology data derived from OBIA were used to examine the iceberg size and distribution within the fjord. Here, ice mélange is typically shorter and more densely packed with icebergs in the winter, but is longer and filled with sea ice and/or unresolvable iceberg pieces during the summer. Ice mélange jams often coincided when 30% ($\pm$12%) of all icebergs were within $\sim$5 km of the glacier terminus.

The terminus area data were split into discrete transects, and were compared with one another, termed as calving style. Calving style of the transects varied inter-seasonally, but no two portions of the glacier ever correlated negatively, indicating that iceberg calving occurs along the terminus nearly simultaneously. However, the calving style varied almost randomly in some areas of the glacier terminus during ice mélange jams, which coincides with winter, a time when calving is slow relative to the summer and early fall seasons at HG. Both bed topography datasets were distinctly different, and neither agreed in terms of HG's terminus and stability. An equilibrium was evident when plotting terminus position as frequency, but did not correlate to a topographic high, low or slope in either bed topography dataset. Downslope wind events (DWE) did not dictate the extent or rigidity of the ice mélange. Subsurface ocean temperatures recorded by moorings showed that the ocean waters during the winter are well above freezing; variation in their winter highs do not correspond to a change in calving rate.

More often than not, ice mélange jamming did not correlate to iceberg calving events at HG; the potential for a delayed response was examined by lagging the events up to 30 days, which yielded only less significant correlations. Here, a shorter jam (2 days) observed with a fully extended ice mélange ($\sim$26 km) indicated that short-term jams can occur, and are likely related to the arrangement and density of icebergs. Jams spanning multiple days do not necessarily impact iceberg calving, though longer jams (up to 35 days) were likely to occur in winter, and when icebergs are clustered within 5 km of the glacier terminus. $\sim$11-16 days jams occurred in all seasons. SST and seasonality were the two clearest signals in terms of controls on the glacier terminus, following the theories of acceleration and subsequent calving being driven by seasonal melt.

References

Amundson, J., Fahnestock, M., Truffer, M., Brown, J., Lüthi, M., & Motyka, R. (2010). Ice mélange dynamics and implications for terminus stability, jakobshavn isbræ, greenland. *J. Geophys. Res.: Earth Surface (2003–2012)*, 115(F1).

Amundson, J. & Truffer, M. (2010). A unifying framework for iceberg-calving models. *J. Glaciol.*, 56(199), 822–830.

Amundson, J., Truffer, M., Lüthi, M., Fahnestock, M., West, M., & Motyka, R. (2008). Glacier, fjord, and seismic response to recent large calving events, jakobshavn isbræ, greenland. *Geophysical Research Letters*, 35(22).

Bamber, J., Griggs, J., Hurkmans, R., Dowdeswell, J., Gogineni, S., Howat, I., Mouginot, J., Paden, J., Palmer, S., Rignot, E., et al. (2013). A new bed elevation dataset for greenland. *The Cryosphere*, 7(2), 499–510.

Bartholomew, I., Nienow, P., Mair, D., Hubbard, A., King, M. A., & Sole, A. (2010). Seasonal evolution of subglacial drainage and acceleration in a greenland outlet glacier. *Nature Geoscience*, 3(6), 408–411.

Bassis, J. & Jacobs, S. (2013). Diverse calving patterns linked to glacier geometry. *Nature Geoscience*, 6(10), 833–836.

Benn, D. I., Hulton, N. R., & Mottram, R. H. (2007). 'calving laws','sliding laws' and the stability of tidewater glaciers. *Annals of glaciology*, 46(1), 123–130.

Bevan, S., Luckman, A., Khan, S., & Murray, T. (2015). Seasonal dynamic thinning at helheim glacier. *Earth and Planetary Science Letters*, 415, 47–53.

Chauché, N., Hubbard, A., Gascard, J.-C., Box, J., Bates, R., Koppes, M., Sole, A., Christoffersen, P., & Patton, H. (2014). Ice–ocean interaction and calving front morphology at two west greenland tidewater outlet glaciers. *The Cryosphere*, 8(4), 1457–1468.

Church, J. A., Clark, P. U., Cazenave, A., Gregory, J. M., Jevrejeva, S., Levermann, A., Merrifield, M., Milne, G., Nerem, R., Nunn, P., et al. (2013). *Sea level change*. Technical report, PM Cambridge University Press.

Csatho, B. M., Schenk, A. F., van der Veen, C. J., Babonis, G., Duncan, K., Rezvanbehbahani, S., van den Broeke, M. R., Simonsen, S. B., Nagarajan, S., & van Angelen, J. H. (2014). Laser altimetry reveals complex pattern of greenland ice sheet dynamics. *Proceedings of the National Academy of Sciences*, 111(52), 18478–18483.

Davis, J. L., De Juan, J., Nettles, M., Elosegui, P., & Andersen, M. L. (2014). Evidence for non-tidal diurnal velocity variations of helheim glacier, east greenland. *J. Glaciol.*, 60(224), 1169–1180.

Enderlin, E., Howat, I., Jeong, S., Noh, M., Angelen, J., & Broeke, M. (2014). An improved mass budget for the greenland ice sheet. *Geophys. Res. Lett.*, 41(3), 866–872.

Enderlin, E. M. & Howat, I. M. (2013). Submarine melt rate estimates for floating termini of greenland outlet glaciers (2000–2010). *J. Glaciol.*, 59(213), 67–75.

Hanson, B. & Hooke, R. L. (2000). Glacier calving: a numerical model of forces in the calving-speed–water-depth relation. *J. Glaciol.*, 46(153), 188–196.

Harden, B. E., Straneo, F., & Sutherland, D. A. (2014). Moored observations of synoptic and seasonal variability in the east greenland coastal current. *J. Geophys. Res.: Oceans*, 119(12), 8838–8857.

Holland, D., Thomas, R., De Young, B., Ribergaard, M., & Lyberth, B. (2008). Acceleration of jakobshavn isbrae triggered by warm subsurface ocean waters. *Nature Geoscience*, 1(10), 659–664.

Howat, I., Joughin, I., Tulaczyk, S., & Gogineni, S. (2005). Rapid retreat and acceleration of helheim glacier, east greenland. *Geophys. Res. Lett.*, 32(22).

Howat, I. M., Box, J. E., Ahn, Y., Herrington, A., & McFadden, E. M. (2010). Seasonal variability in the dynamics of marine-terminating outlet glaciers in greenland. *J. Glaciol.*, 56(198), 601–613.

Howat, I. M., Joughin, I., & Scambos, T. A. (2007). Rapid changes in ice discharge from greenland outlet glaciers. *Science*, 315(5818), 1559–1561.

Hughes, T. (1986). The jakobshanvs effect. *Geophysical Research Letters*, 13(1), 46–48.

Hughes, T. J. (1992). Theoretical calving rates from glaciers along ice walls grounded in water of variable depths. *Journal of Glaciology*, 38(129), 282.

James, T. D., Murray, T., Selmes, N., Scharrer, K., & O'Leary, M. (2014). Buoyant flexure and basal crevassing in dynamic mass loss at helheim glacier. *Nature Geoscience*, 7(8), 593–596.

Joughin, I., Abdalati, W., & Fahnestock, M. (2004). Large fluctuations in speed on greenland's jakobshavn isbrae glacier. *Nature*, 432(7017), 608–610.

Joughin, I., Howat, I., Alley, R., Ekstrom, G., Fahnestock, M., Moon, T., Nettles, M., Truffer, M., & Tsai, V. (2008a). Ice-front variation and tidewater behavior on helheim and kangerdlugssuaq glaciers, greenland. *J. Geophys. Res.: Earth Surface (2003–2012)*, 113(F1).

Joughin, I., Howat, I. M., Fahnestock, M., Smith, B., Krabill, W., Alley, R. B., Stern, H., & Truffer, M. (2008b). Continued evolution of jakobshavn isbrae following its rapid speedup. *Journal of Geophysical Research: Earth Surface*, 113(F4).

Joughin, I., Smith, B., Howat, I., & Scambos, T. (2011, updated 2014). Measures greenland ice velocity: selected glacier site velocity maps from insar, version 1. [ecoast-66.50n]. *Boulder, Colorado, USA: NASA DAAC at the National Snow and Ice Data Center*, 10. Accessed 2016-02-08.

Kuo, C. & Dennin, M. (2013). Buckling-induced jamming in channel flow of particle rafts. *Physical Review E*, 87(3), 030201.

Luckman, A. & Murray, T. (2005). Seasonal variation in velocity before retreat of jakobshavn isbræ, greenland. *Geophysical Research Letters*, 32(8).

Luckman, A., Murray, T., De Lange, R., & Hanna, E. (2006). Rapid and synchronous ice-dynamic changes in east greenland. *Geophysical Research Letters*, 33(3).

Meier, M. & Post, A. (1987). Fast tidewater glaciers. *J. Geophys. Res.: Solid Earth (1978–2012)*, 92(B9), 9051–9058.

Meier, M. F., Dyurgerov, M. B., Rick, U. K., O'Neel, S., Pfeffer, W. T., Anderson, R. S., Anderson, S. P., & Glazovsky, A. F. (2007). Glaciers dominate eustatic sea-level rise in the 21st century. *Science*, 317(5841), 1064–1067.

Moon, T., Joughin, I., Smith, B., Broeke, M. R., Berg, W. J., Noël, B., & Usher, M. (2014). Distinct patterns of seasonal greenland glacier velocity. *Geophysical research letters*, 41(20), 7209–7216.

Morlighem, M., Rignot, E., Mouginot, J., Seroussi, H., & Larour, E. (2014). Deeply incised submarine glacial valleys beneath the greenland ice sheet. *Nature Geoscience*, 7(6), 418–422.

Motyka, R. J., Truffer, M., Fahnestock, M., Mortensen, J., Rysgaard, S., & Howat, I. (2011). Submarine melting of the 1985 jakobshavn isbræ floating tongue and the triggering of the current retreat. *Journal of Geophysical Research: Earth Surface*, 116(F1).

Murray, T., Scharrer, K., Selmes, N., Booth, A., James, T., Bevan, S., Bradley, J., Cook, S., Llana, L. C., Drocourt, Y., et al. (2015). Extensive retreat of greenland tidewater glaciers, 2000-2010. *Arctic, Antarctic, and Alpine Research*, 47(3), 427–447.

Nettles, M. & Ekström, G. (2010). Glacial earthquakes in greenland and antarctica. *Annual Review of Earth and Planetary Sciences*, 38(1), 467.

Nettles, M., Larsen, T., Elósegui, P., Hamilton, G. S., Stearns, L. A., Ahlstrøm, A. P., Davis, J., Andersen, M., de Juan, J., Khan, S. A., et al. (2008). Step-wise changes in glacier flow speed coincide with calving and glacial earthquakes at helheim glacier, greenland. *Geophysical Research Letters*, 35(24).

Nick, F., Luckman, A., Vieli, A., Van der Veen, C. J., Van As, D., Van de Wal, R., Pattyn, F., Hubbard, A., & Floricioiu, D. (2012). The response of petermann glacier, greenland, to large calving events, and its future stability in the context of atmospheric and oceanic warming. *J. Glaciol.*, 58(208), 229–239.

Nick, F., Van der Veen, C., Vieli, A., & Benn, D. (2010). A physically based calving model applied to marine outlet glaciers and implications for the glacier dynamics. *J. Glaciol.*, 56(199), 781–794.

Nick, F. M., Vieli, A., Howat, I. M., & Joughin, I. (2009). Large-scale changes in greenland outlet glacier dynamics triggered at the terminus. *Nature Geoscience*, 2(2), 110–114.

Oerlemans, J. (2005). Extracting a climate signal from 169 glacier records. *Science*, 308(5722), 675–677.

Pelto, M. & Warren, C. (1991). Relationship between tidewater glacier calving velocity and water depth at the calving front. *Ann. Glaciol.*, 15, 115–118.

Peters, I., Amundson, J., Cassotto, R., Fahnestock, M., Darnell, K., Truffer, M., & Zhang, W. (2015). Dynamic jamming of iceberg-choked fjords. *Geophys. Res. Lett.*, 42(4), 1122–1129.

Reeh, N., Thomsen, H., Higgins, A., & Weidick, A. (2001). Sea ice and the stability of north and northeast greenland floating glaciers. *Ann. Glaciol.*, 33(1), 474–480.

Rignot, E., Koppes, M., & Velicogna, I. (2010). Rapid submarine melting of the calving faces of west greenland glaciers. *Nature Geoscience*, 3(3), 187–191.

Rignot, E. & MacAyeal, D. (1998). Ice-shelf dynamics near the front of the filchner-ronne ice shelf, antarctica, revealed by sar interferometry. *Journal of Glaciology*, 44(147).

Schild, K. & Hamilton, G. (2013). Seasonal variations of outlet glacier terminus position in greenland. *J. Glaciol.*, 59(216), 759–770.

Schild, K. M. (2011). *Terminus Changes of Tidewater Outlet Glaciers in Greenland: Environmental Controls and Links to Glacial Earthquakes*. PhD thesis, University of Maine.

Slater, D., Nienow, P., Cowton, T., Goldberg, D., & Sole, A. (2015). Effect of near-terminus subglacial hydrology on tidewater glacier submarine melt rates. *Geophys. Res. Lett.*, 42(8), 2861–2868.

Sohn, H.-G., Jezek, K. C., & van der Veen, C. J. (1998). Jakobshavn glacier, west greenland: 30 years of spaceborne observations. *Geophysical Research Letters*, 25(14), 2699–2702.

Stearns, L. & Hamilton, G. (2007). Rapid volume loss from two east greenland outlet glaciers quantified using repeat stereo satellite imagery. *Geophys. Res. Lett.*, 34(5).

Stearns, L. A., Hamilton, G. S., van der Veen, C., Finnegan, D., O'Neel, S., Scheick, J., & Lawson, D. (2015). Glaciological and marine geological controls on terminus dynamics of hubbard glacier, southeast alaska. *Journal of Geophysical Research: Earth Surface*, 120(6), 1065–1081.

Sundal, A., Shepherd, A., Van Den Broeke, M., Van Angelen, J., Gourmelen, N., & Park, J. (2013). Controls on short-term variations in greenland glacier dynamics. *Journal of Glaciology*, 59(217), 883–892.

Sutherland, D., Roth, G., Hamilton, G., Mernild, S., Stearns, L., & Straneo, F. (2014). Quantifying flow regimes in a greenland glacial fjord using iceberg drifters. *Geophys. Res. Lett.*, 41(23), 8411–8420.

Sutherland, D. & Straneo, F. (2012). Estimating ocean heat transports and submarine melt rates in sermilik fjord, greenland, using lowered acoustic doppler current profiler (ladcp) velocity profiles. *Ann. Glaciol.*, 53(60), 50–58.

Thomas, R. H., Abdalati, W., Frederick, E., Krabill, W. B., Manizade, S., & Steffen, K. (2003). Investigation of surface melting and dynamic thinning on jakobshavn isbrae, greenland. *J. Glaciol.*, 49(165), 231–239.

Van der Veen, C. (1996). Tidewater calving. *J. Glaciol.*, 42(141), 375–385.

Van der Veen, C. (2002). Calving glaciers. *Progress in Physical Geography*, 26(1), 96–122.

Van der Veen, C. J. (2007). Fracture propagation as means of rapidly transferring surface meltwater to the base of glaciers. *Geophysical Research Letters*, 34(1).

Van der Veen, C. J., Plummer, J., & Stearns, L. (2011). Controls on the recent speed-up of jakobshavn isbræ, west greenland. *Journal of Glaciology*, 57(204), 770–782.

Van der Veen, C. J. & Whillans, I. (1989). Force budget: I. theory and numerical methods. *J. Glaciol.*, 35(119), 53–60.

Velicogna, I. (2009). Increasing rates of ice mass loss from the greenland and antarctic ice sheets revealed by grace. *Geophysical Research Letters*, 36(19).

Venteris, E. R. (1999). Rapid tidewater glacier retreat: a comparison between columbia glacier, alaska and patagonian calving glaciers. *Global and Planetary Change*, 22(1), 131–138.

Walter, J., Box, J., Tulaczyk, S., Brodsky, E., Howat, I., Ahn, Y., & Brown, A. (2012). Oceanic mechanical forcing of a marine-terminating greenland glacier. *Ann. Glaciol.*, 53(60), 181–192.

Zwally, H. J., Abdalati, W., Herring, T., Larson, K., Saba, J., & Steffen, K. (2002). Surface melt-induced acceleration of greenland ice-sheet flow. *Science*, 297(5579), 218–222.

Zwally, H. J., Jun, L., Brenner, A. C., Beckley, M., Cornejo, H. G., DiMARZIO, J., Giovinetto, M. B., Neumann, T. A., Robbins, J., Saba, J. L., et al. (2011). Greenland ice sheet mass balance: distribution of increased mass loss with climate warming; 2003–07 versus 1992–2002. *J. Glaciol.*, 57(201), 88–102.